도시계획학박사 학위논문

A prognostic estimation of limited-visibility risk for honey bee (*Apis mellifera*) under increasing emission of anthropogenic particulate matter

대기 중 미세먼지의 증가로 인한 꿀벌의 시계 제한 예측

2023년 8월

서울대학교 대학원

환경계획학과 환경관리전공

조 유 리

A prognostic estimation of limited-visibility risk for honey bee (*Apis mellifera*) under increasing emission of anthropogenic particulate matter

대기 중 미세먼지의 증가로 인한 꿀벌의 시계 제한 예측

지도 교수 정 수 종

이 논문을 도시계획학박사 학위논문으로 제출함
2023년 8월

서울대학교 대학원
환경계획학과 환경관리전공
조 유 리

조유리의 도시계획학박사 학위논문을 인준함
2023년 8월

위 원 장 윤 순 진 (인)

부위원장 최 창 용 (인)

위 원 박 찬 열 (인)

위 원 장 동 영 (인)

위 원 정 수 종 (인)

Abstract

A prognostic estimation of limited-visibility risk for honey bee (*Apis mellifera*) under increasing emission of anthropogenic particulate matter

Yoori Cho

Department of Environmental Planning

The Graduate School of Environmental Studies

Seoul National University

Among numerous insect pollinators, bees are widely recognized as the primary agents and contributors to pollination services. However, the global bee population is declining due to various biotic and abiotic factors. Anthropogenic stressors have been identified and investigated, as they pose a significant threat to bees and their foraging activities. These stressors include insufficient food resources, pathogens, parasites, and pesticide use. Additionally, poor air quality can negatively impact bee foraging. The increased concentration of anthropogenic aerosols leads to excessive scattering of electromagnetic radiation, resulting in a reduction of the degree linear polarization (DoLP) of the skylight. Honey bees (*Apis mellifera*) can navigate by utilizing the polarization pattern surrounding the sun, which is considered their primary orientation mechanism. However, to achieve optimal orientation, honey bees require at least 15% DoLP in an unobstructed area of the overhead sky during flight.

The mass scattering efficiency for most aerosol types with particles

smaller than 1 μm is greater than that with larger particles. The atmospheric loading of fine mode particles, represented by PM2.5 (airborne particles with aerodynamic diameters less than 2.5 μm) mass concentration, should exhibit a strong correlation with the celestial DoLP. Consequently, decreases in the DoLP, can adversely affect the foraging behavior of bee pollinators that rely on polarized light cues for visual navigation when the Sun is obscured. However, there is limited empirical evidence on whether poor air quality indeed affects the foraging performance of honey bees. This study aims to project the potential increase in the spatio-temporal magnitude of limited-visibility risk for honey bees (*Apis mellifera*) resulting from a reduction in DoLP due to increasing PM2.5 emissions. For this research purpose, field monitoring of a colony, ground observation of the DoLP, and future projections of the clear-sky visibility for honey bees were conducted.

By monitoring the foraging activities of honey bee colonies using a radio-frequency identification system, it was demonstrated that clear increases in the average duration of honey bee foraging during and after a severe air pollution event compared to the pre-event period. The average foraging duration of honey bees during the event increased by 32 minutes compared to the pre-event conditions, indicating a 71% increase in foraging time. Furthermore, the average foraging duration measured after the event did not recover to its pre-event level. Average foraging trip durations increased as PM2.5 mass concentration increased, regardless of the occurrence of a heavy pollution event. The influence of an optical property (Depolarization Ratio, DR) of dominant particulate matter in the atmosphere and the level of air pollution (PM2.5 mass concentration) on foraging trip duration was further investigated. The results illustrated that both DR and PM2.5 mass concentration have a significant effect on honey bee foraging trip duration. Foraging trip duration increases with decreasing DR, while it increases with increasing PM2.5 mass concentration. These findings from the field monitoring are essential because longer foraging trips increase the likelihood of encountering other stressors, such as insecticide residue and parasites, while searching for food and navigating between their home and resources.

Additionally, to evaluate the potential increase of limited-visibility risks faced by honey bees due to PM2.5 emissions in the future, a comprehensive investigation was conducted. Initially, a relationship between PM2.5 mass concentration and DoLP was quantified through long-term ground monitoring of linear polarization. This involved utilizing a digital all-sky imaging system for ground-based imaging polarimetry. Cloud-free full-sky images were collected during two distinct periods, spanning from 2018 to 2019 and from 2020 to 2021. The celestial DoLP was then determined by analyzing the Stokes parameters associated with each observation. By developing a statistical parameterization capturing the relationship between PM2.5 mass concentrations and DoLP values, the corresponding PM2.5 concentrations required to meet the navigational DoLP threshold of honey bees were calculated. The cases were divided into two categories: the most probable DoLP over the sky presented to bees, which was assumed to be close to the average DoLP, and the higher-end DoLP under cloud-free sky conditions, which was assumed to be the maximum DoLP. In other words, for a given PM2.5 mass concentration, the available DoLP perceived by the bee may fall between the average and the maximum DoLPs in their overhead sky. Thus, for future estimations, the average and maximum DoLP values for each observation were utilized to determine the likely range of corresponding PM2.5 concentrations that met the navigational threshold.

Subsequently, the threshold PM2.5 mass concentrations were applied to the projected global distribution of PM2.5 mass concentrations for the year 2050, as simulated by the ECHAM5/MESSy atmospheric climate chemistry model. This model was chosen to evaluate the potential

consequences of the absence of mitigation efforts for air quality. It assumes the continuation of national air pollution mitigation policies established in 2010, while considering anticipated population growth and economic development. Then, "risk hotspot" regions (one hotspot is 1.1° by 1.1° in latitude and longitude) were determined, where honey bees are projected to experience limited visibility for at least one day in 2050. Finally, the spatial extent of risk hotspots and the frequency of limited-visibility days (LVD) per hotspot (i.e., the number of LVD) were assessed at the global, regional, and national scales annually and seasonally. Additionally, the expected increases in both the extent of risk hotspots and the frequency of LVD relative to the baseline year of 2010, as simulated by the model, were estimated. The results showed that India and China will experience significant increases in the area under limited-visibility risk and the frequency of limited-visibility days. In India, even under a higher-end estimation, the area under limited-visibility risk will increase from 0.06 million (M) km^2 in 2010 to 0.75 M km^2 in 2050. Moreover, an increased frequency of limited-visibility days is expected across nearly every part of India. In China, for an area of 2 M km2 under limited-visibility risk in 2050, 1.1 M km^2 will experience an increased frequency of limited-visibility days between 2010 and 2050.

The delayed duration of foraging trips and the increased risk of limited visibility due to deteriorating air quality, as identified in this study, demonstrate that poor air quality can serve as a significant stressor alongside existing threats to pollinator-plant interactions, including pesticide use, habitat destruction, parasites, and pathogens. These findings suggest that mitigating anthropogenic air pollution can play a crucial role in safeguarding plant-pollinator interactions, particularly in the world's top two producers of pollinator-dependent crops.

Keywords : Biodiversity, Pollination service, *Apis mellifera*, PM2.5, Degree of linear polarization, Air quality projection
Student Number : 2015-31317

Table of Contents

List of Tables

List of Figures

1. Introduction

1.1 Ecological significance of pollination services

Pollination ecology, particularly focusing on insect pollinators, has been extensively investigated in the scientific community due to the recognition of pollination as a prime example of an ecosystem service. This recognition acknowledges not only the economic advantages but also the fundamental life-sustaining processes it provides (Daily 2000; Ricketts *et al.* 2008; Knight *et al.* 2018). Consequently, numerous interdisciplinary studies have been conducted to evaluate the worldwide reliance on insect-pollinated agriculture and the resulting economic vulnerability caused by declines in pollinator populations (Potts *et al.* 2016; Knight *et al.* 2018). These studies have estimated that over 70% of globally significant food crop types benefit from animal pollinators (Klein *et al.* 2007). Recent estimations indicate that the annual global agricultural benefit derived from crop pollination by insect pollinators is approximately $400 billion (Lautenbach *et al.* 2012).

Although these impressive figures are still considered to underestimate the total benefits of pollination services, quantifying these benefits in monetary terms has proven useful in supporting the conservation of ecosystem services in the context of increasing demands for food security (Breeze *et al.* 2016; Khalifa *et al.* 2021). However, economic measures have faced criticism for their anthropocentric perspective (Farber *et al.* 2002; Chee 2004). Many argue that we should recognize the non-economic and non-market values of pollination services, as nature's usefulness to humans is not its sole manifestation (Nabhan & Buchmann 1997; Breeze *et al.* 2016). This perspective differs to some extent from the recognition that pollinators also provide aesthetic and cultural value, which are often regarded as non-market benefits of pollination services (Hanley *et al.* 2015). However, even these non-market benefits rely on the way people utilize them, reflecting an anthropocentric viewpoint.

Beyond the anthropocentric perspective, approximately 87.5% of global flowering plant species depend on insect pollination for their reproduction (Ollerton *et al.* 2011). In other words, if pollination declines, ecological processes related to primary production will be supported by only 12.5% of the current flowering plant species on Earth. Such a loss of pollination could result in the simultaneous degradation of other ecosystem services to some extent (Christmann 2019). Therefore, a global overarching goal should be to benefit not only human communities but also the diverse biological communities that rely on the multitude of pollinators (Allen-Wardell *et al.* 1998). Ultimately, human well-being is inseparable from the conservation of ecosystem functions as a whole (Potts *et al.* 2016). In this regard, pollination services hold not only economic significance but also ecological significance.

As previously stated, insect pollinators, as primary consumers in our ecosystem, play a crucial role in the reproduction of nearly all flowering plants. However, sudden collapses in pollinator populations can lead to the extinction of suitable habitats for a wide range of species (Christmann 2019). The loss of vegetation can trigger cascading effects, resulting in the extinction of species reliant on those habitats and posing a threat to the resilience of ecosystem functions. These functions can include mitigating the effects of climate change, which is one of the most pressing ecological challenges of our time. For instance, the understory vegetation layer in ecosystems harbors more than 90% of plant species and represents the majority of floristic diversity, with insect pollinators being responsible for their reproduction (Gilliam 2007; Proctor *et al.* 2012). While understory vegetation may not contribute the most to the total productivity of a forest ecosystem, it enhances variations in the ecosystem's structure and composition (Kim *et al.* 2016). In temperate forest ecosystems, understory vegetation plays a significant role in mitigating climate change by increasing net ecosystem production and carbon input into the soil (Dirnböck *et al.* 2020). Another example involves the role of pollinator-dependent plant species, such as *Rosa canica* and *Cornus mas*, in erosion control (Comino & Marengo 2010). The roots of *Avicennia germinans*, a common pollinator-dependent mangrove species, provide habitat for numerous soil organisms, including mycorrhizal fungi (Vanegas *et al.* 2019). The rapid growth of tulip poplar (*Liriodendron tulipifera* L.), which depends on pollinators, makes it a widely used timber production species with high carbon storage capacity (Baveco *et al.* 2016). Most importantly, insect pollination enhances genetic diversity, leading to the development of genotypes with greater adaptive capacity to climate change (Christmann & Aw-Hassan 2012). However, the wide-ranging contributions of pollinators from the genetic to ecosystem levels also make our ecosystem more vulnerable to pollinator loss.

The loss of biodiversity due to the decline in pollination services reduces the functional diversity of organisms that help the entire ecosystem adapt to and mitigate the effects of increasing environmental disturbances, including climate change. This, in turn, can accelerate climate warming, resulting in population declines of various species, including pollinators. From a biodiversity perspective, pollination is receiving increasing recognition. The Kunming-Montreal Global Biodiversity Framework (GBF), agreed upon at the 15th meeting of the Conference of Parties to the UN Convention on Biological Diversity in

2022, emphasizes the urgent need for international support and commitment to conserve increasingly threatened biodiversity (Convention on Biological Diversity, 2022). Target 3 of the framework sets a highly ambitious goal of protecting a minimum of 30% of land and ocean areas by 2030, including the protection of pollinator habitats (Arneth *et al.* 2023). Additionally, Target 11 of the GBF specifically aims not only to maintain but also to improve ecosystem functioning, including pollination (Antonelli 2023).

In light of the aforementioned examples, it is evident that pollination services, which contribute to maintaining biodiversity in our ecosystem, play a vital role in sustaining ecological functions beyond plant reproduction, which is commonly considered its primary contribution (Christmann 2019). This contribution cannot simply be categorized as aesthetic or cultural benefits, as discussed earlier. While an increasing number of studies highlight the importance of including non-market values of pollination services (Hanley *et al.* 2015; Christmann 2019), many of these studies are still limited to assessing values that people can acknowledge and appreciate by utilizing them, such as their role in controlling and mitigating environmental disturbances (Mwebaze *et al.* 2018; Stout *et al.* 2019).

Based on literature review, Figure 1 presents a straightforward schematic depiction of pollination services, which serve as a vital supporting service in the ecosystem, contributing to the enhancement of biodiversity and consequential ecosystem functioning.

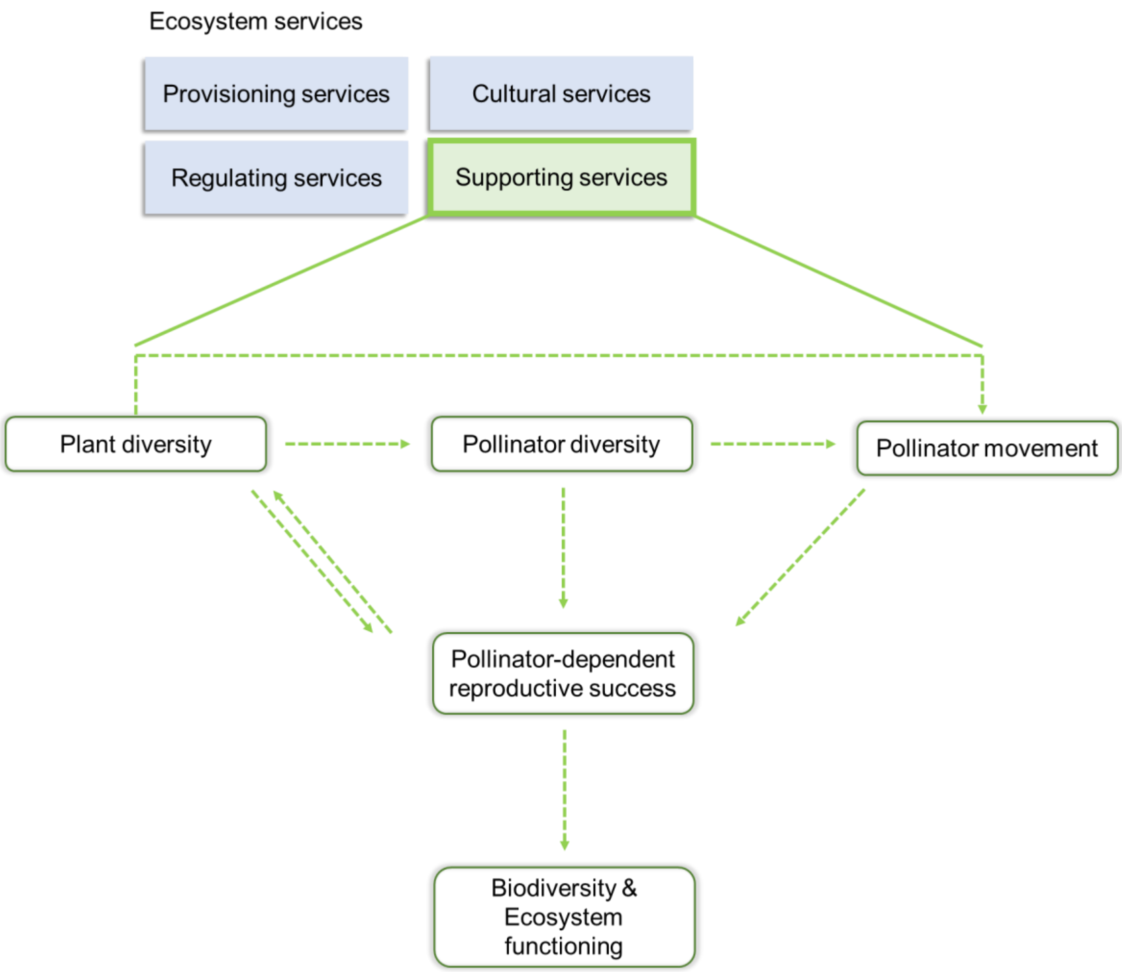

Figure 1. Schematic depiction of pollination services as a supporting service in the ecosystem, contributing to the enhancement of biodiversity. Partially redrawn from Hadley & Betts 2012.

1.2 Human impacts on bee foraging

1.2.1 Biotic and abiotic stressors to bee foraging

Among the various insect pollinators, bees are recognized as key agents and contributors to pollination services (Powney *et al.* 2019). However, global bee populations are declining due to a combination of biotic and abiotic factors (Ricketts *et al.* 2008; Klein *et al.* 2017; Cappa *et al.* 2019). These factors can be attributed to anthropogenic stressors, which potentially affect the energy budget of bees and consequently result in reduced foraging performance (Bordier *et al.* 2018). The efficiency of pollination services heavily relies on the effective foraging behavior of bees (Goulson & Nicholls 2022). Anthropogenic stressors that pose threats to bee foraging have been extensively identified and investigated (Potts et al. 2010; Klein et al. 2017). These stressors can be broadly categorized into two groups: biotic and abiotic. Abiotic stressors encompass the use of agrochemicals, exposure to pollutants such as heavy metals, the expansion of intensive agriculture, and increasing heat stress. Biotic stressors, on the other hand, involve disease infections caused by parasites and pathogens. The combined impact of these stressors can lead to the degradation of pollination services through reduced foraging efficiency and colony collapse (Klein *et al.* 2017).

The use of agrochemicals, specifically pesticides, stands out as the most controversial and extensively studied factor contributing to the global bee crisis among the abiotic stressors (Goulson *et al.* 2015; Lundin *et al.* 2015; Woodcock *et al.* 2017). Regional and global investigations on pesticide residues in honey samples have demonstrated that bees are exposed to multiple pesticides in the field (Sanchez-Bayo & Goka 2014; Mitchell *et al.* 2017). The impacts of common pesticide exposure on bee foraging have been examined, particularly in terms of the navigational ability of forager bees. Henry *et al*. found that sublethal doses of neonicotinoids decreased the success of honey bee (*Apis mellifera*) foraging by measuring the homing probability of forager bees (Henry *et al.* 2012). Similarly, Jin *et al.* found that the neonicotinoid clothianidin disrupted the navigation of *Osmia cornuta* species (Jin *et al.* 2015). Numerous studies have also demonstrated impairments in the flight ability of honey bees after exposure to common pesticides (Tosi *et al.* 2017; Colin *et al.* 2019). The impacts of insecticides on foraging behavior have been widely studied in other bee species as well (Gels *et al.* 2002; Stanley *et al.* 2015).

Pollutants can also influence the foraging behavior of bees. Heavy metals, such as copper and lead, present in roadside dust have been found to reduce the frequency of foraging trips per bee (Phillips *et al.* 2021). In a laboratory experiment, honey bees exposed to manganese showed increased foraging trip duration (Søvik *et al.* 2015). Similarly, in another laboratory experiment, it was demonstrated that diesel exhaust affected learning and memory in honey bees (Girling *et al.* 2013; Goulson *et al.* 2015; Fuentes *et al.* 2016; Reitmayer *et al.* 2019). The expansion of intensive agriculture, distant from natural habitats, has increased the foraging distance of bees, leading to reduced food availability and increased nutritional stress (Ricketts *et al.* 2008; Kennedy *et al.* 2013; Danner *et al.* 2016; Klein *et al.* 2017). Although there are limited studies specifically examining the effects of rising temperatures due to climate change on bee foraging, it is likely that global warming will impact foraging efficiency (Goulson & Nicholls 2022). Overheating of the nest forces worker bees to spend more energy on cooling the temperature inside the nest rather than foraging (Johnson 2002). Such labor reallocation would eventually reduce the frequency of foraging activity.

Biotic stressors encompass diseases transmitted by parasites and pathogens. The spread of diseases through shared floral resources and contact between bees has become a growing concern for pollinator conservation (Koch *et al.* 2017). The transmission of diseases not only within species but also between different species accelerates their spread (Potts *et al.* 2010; Fürst *et al.* 2014; Koch *et al.* 2017). *Varroa destructor* and *Nosema ceranae* are the most common parasites implicated in the recent global collapse of domesticated honey bees (Potts *et al.* 2010; Wilfert *et al.* 2016). Bees infested with parasites exhibit lower foraging efficiency and contribute less to pollination (Lach *et al.* 2015). The widespread presence of Deformed Wing Virus (DWV), carried by Varroa, often leads to wing deformities in bees, resulting in increased foraging stress and reduced flight performance (Wells *et al.* 2016; Roberts *et al.* 2017). The human-altered viral landscape is now common, leading to the prevalence of sublethal and lethal diseases in pollinator communities.

1.2.2 Interactions between the stressors

Although our understanding is limited, an increasing number of studies are investigating the interactions between different stressors (Goulson *et al.* 2015; Goulson & Nicholls 2022). The impact of flupyradifurone, a new synthetic pesticide, on the reduction of flight success in honey bees is more pronounced when the bees are experiencing nutritional stress (Tong *et al.* 2019). Pesticide exposure can suppress the immune system of honey bees, facilitating the spread of viral pathogens such as DWV (Di Prisco *et al.* 2013). While some studies did not directly examine the interplay of stressors, we can still predict how one stressor can synergistically interact with others. For instance, *Nosema* species, a common pathogen infecting honey bees, is less prevalent in low temperatures (Gisder *et al.* 2010), suggesting an increased pathogen infectivity under rising temperatures. Dietary stress, often accompanied by starvation due to limited floral resources caused by climate change and intensive farming, as discussed earlier, can make bees more vulnerable to disease infections (Erler *et al.* 2014; Goulson *et al.* 2015). Spatial and temporal mismatches between plant and pollinator phenology can exacerbate nutritional stress in bees (Fisogni *et al.* 2020). Furthermore, floral diversity itself holds the potential to provide antimicrobial effects through metabolites in floral resources, enhancing the immunity of bees foraging on those resources (Erler *et al.* 2014). The combination of nutritional stress and pathogen stress leads to precocious foraging in bees (i.e., forage early in age), contributing to a rapid decline in colony population (Perry *et al.* 2015).

1.3 Air quality as an environmental stressor

While a significant amount of research has been conducted on bee population decline, with a focus on the aforementioned stressors, only a limited number of studies have examined the impacts of air quality on pollinator activity. Recently, progress has been made in laboratory studies investigating the relationship between olfactory learning in honey bees and air pollution (Girling *et al.* 2013; Reitmayer *et al.* 2019). However, the potential effects of poor air quality on "honey bee vision," which is crucial for stable foraging (Srinivasan 2011), have yet to be investigated. Of Note, other than bee species, the effects of poor air quality on foraging duration of butterfly species have been investigated (Liu *et al.* 2021), as well as the spatial association between PM2.5 and geographical flight ranges of nocturnally migrating birds worldwide (La Sorte *et al.* 2022). Additionally, the physiological impacts of poor air quality on butterfly populations have been studied, along with bird populations (Tan *et al.* 2018; Kozlov 2022) along with bird populations (Sanderfoot & Holloway 2017; Liang *et al.* 2020).

1.3.1 Visual navigation of honey bees (*Apis mellifera*)

Though invisible to the human eye, the polarization pattern of skylight, a major characteristic of electromagnetic radiation (Chen *et al.* 2020), serves as a reliable compass for nearly all insect species (Foster *et al.* 2014). While incoming radiation is initially unpolarized, it becomes linearly polarized upon scattering by atmospheric molecules (Emde *et al.* 2010). It is empirically known that insect species relying on polarized light for visual navigation become disoriented during episodes of air pollution, such as volcanic eruptions and wildfire outbreaks, as the degree of linear polarization (DoLP) is highly influenced by atmospheric conditions (Hegedüs *et al.* 2007a). Although clouds are not considered pollutants, a sky obscured by scattered clouds can limit the "polarotactic response" of insects (Henze & Labhart 2007).

One such insect species is the honey bee (Apis mellifera). In this dissertation, the term "honey bee" refers specifically to *Apis mellifera*. Honey bees possess strongly polarization-sensitive photoreceptors (Kelber & Somanathan 2019) and use polarized light patterns to orient themselves and navigate between food sources and their hive (Rossel & Wehner 1982; Kraft *et al.* 2011; Evangelista *et al.* 2014). Even when the sun is obstructed by clouds, honey bees can still navigate by utilizing the polarization pattern surrounding the sun, which is considered their primary orientation mechanism (Dovey *et al.* 2013).

Therefore, it is crucial to ensure that honey bees are provided with sufficient polarized skylight information for their navigation. The threshold value for the DoLP that honey bees can perceive can be as low as 10% (Brines & Gould 1982). However, to achieve optimal orientation, honey bees require at least 15% DoLP (referred to as the navigational threshold) in an unobstructed area of the overhead sky during flight (Brines & Gould 1982; Rossel & Wehner 1984; Henze & Labhart 2007; Von Frisch 2013).

1.3.2 PM2.5 and the degree of linear polarization (DoLP) of skylight

Airborne aerosols have both direct and indirect effects on climate. Directly, they can impact the climate through the extinction (scattering and absorption) of solar and terrestrial radiation (Emde *et al.* 2010). Indirectly, aerosols can interact with clouds, leading to aerosol-cloud-climate interactions (Mahowald 2011). Anthropogenic aerosols, particularly fine particulate matter, are more effective in scattering radiation compared to coarse particulate matter like mineral dust. As a result, they contribute to the reduction of incoming solar radiation on Earth, known as global or regional dimming effects, which can be attributed to anthropogenic black and brown carbon (Alpert *et al.* 2005; Streets *et al.* 2006; Wang *et al.* 2009; Schwarz *et al.* 2020). It is well known as global or regional dimming effects to which anthropogenic black and brown carbon are attributable (Schwarz *et al.* 2009; Schwarz *et al.* 2020). The ecological effects of reduced radiation have been investigated in relation to plant growth, including crop production (Burney & Ramanathan 2014; Yue *et al.* 2017; Proctor 2021).

Increased concentrations of anthropogenic aerosols can also reduce the DoLP through excessive scattering of radiation (Hegedüs *et al.* 2007a; Zhao *et al.* 2018). High levels of atmospheric pollution can attenuate the DoLP below the navigational threshold for honey bees, impairing their navigational ability by limiting clear-sky visibility. This not only affects the sustainability of honey bee colonies (Degen *et al.* 2015) but also the pollination services provided by honey bees, which are essential for plant reproduction and ecosystem functioning (Steffan-Dewenter *et al.* 2005; Potts *et al.* 2010; Potts *et al.* 2016).

Under an aerosol-free clean sky, the DoLP is generally strong, but it decreases when non-gaseous particles in the atmosphere scatter skylight (Labhart 1996). In natural scenes, DoLP values typically range from 0 to 50% (Foster *et al.* 2018). Extremely low DoLP values can be observed during heavily polluted conditions, such as massive dust storms with multiple scattering of light (Zhao *et al.* 2018).

Insect species that rely on polarized light for visual navigation, including honey bees, are known to become disoriented during air pollution episodes, such as volcanic eruptions and wildfire outbreaks (Hegedüs *et al.* 2007a). Although clouds are not considered pollutants, a sky shielded by scattered clouds can limit the "polarotactic response" of insects (Henze & Labhart 2007). The DoLP, although a unitless quantity indicating the extent of linear polarization in the total intensity of incoming light (Yan *et al.* 2022), is often expressed as a percentage for easier comprehension.

The scattering of light by particulate matter (PM) increases as the particle size decreases (Hinds 1999). Consequently, light extinction through scattering is primarily governed by fine mode PM, which ranges from 0.1 to 2 μm (Cohan *et al.* 2002). Coarse mode aerosols exhibit relatively lower single scattering albedo compared to fine mode aerosols with the same refractive index (Boesche *et al.* 2006; Gassó & Knobelspiesse 2022). The mass scattering efficiency for most aerosol types with particles larger than 1 μm in radius is lower than that for aerosols with smaller particles at both low and high relative humidity (Latimer & Martin 2019). This can be attributed to the fact that scattering of sunlight per unit mass is most pronounced when the PM size is close to the solar wavelengths of interest, such as near-UV (360-380 nm) to short visible wavelengths (400-500 nm) as considered in this study (Gassó & Knobelspiesse 2022). Excessive scattering results in a reduction of the

DoLP (Zeng *et al.* 2008; Kreuter *et al.* 2010; Gassó & Knobelspiesse 2022). Thus, the microphysical properties of fine mode particles strongly influence the DoLP of a cloudless sky (Boesche *et al.* 2006). Multiple scattering, in particular, depends on particle concentration (Gassó & Knobelspiesse 2022). Therefore, the atmospheric loading of fine mode particles, represented by PM2.5 (airborne particles with aerodynamic diameters less than 2.5 μm) mass concentration, should exhibit a strong correlation with the celestial DoLP.

1.3.3 Importance of understanding the relationship between air quality and foraging activities of honey bee

Overhead sky visibility, referred to as "visibility" hereafter, is analogous to atmospheric visibility to the human eye, as both are primarily influenced by the scattering of light by aerosol particles in the atmosphere (Luan *et al.* 2017; Singh *et al.* 2017; Yao *et al.* 2021). The strong quantitative correlation between atmospheric visibility and the mass concentration of atmospheric particulate matter has already been utilized in a few air quality projections that estimate potential changes in atmospheric visibility in the near future (Martin *et al.* 2014; Ford *et al.* 2018). However, no efforts have been made to predict the future visibility for bees. Due to limited empirical evidence, atmospheric pollution has not been widely recognized as a current or emerging threat to pollinators (Brown *et al.* 2016).

Several modeling studies have predicted the forthcoming impacts of well-known anthropogenic threats, such as habitat loss and climate change, on honey bees (Imbach *et al.* 2017; Otto *et al.* 2018; Cornelissen *et al.* 2019). However, there is a lack of quantitative analyses estimating the impact of air quality on the visual navigation of honey bees.

Poor air quality has the potential to significantly constrain bee foraging and, ultimately, their contribution to pollination. Future projections indicate that air quality in South Asia and Southeast Asia will deteriorate due to climate change-induced air pollution (Kumar *et al.* 2018; Nguyen *et al.* 2019). Moreover, agricultural production in these regions heavily relies on pollination services (Potts *et al.* 2016). While the pollination crisis in the US and Europe has received substantial attention (Goulson *et al.* 2015; Teichroew *et al.* 2017), the attention given to Asian countries facing similar crises has been inadequate. In Asia, the dependency on pollinators for crop yield is increasing (Potts *et al.* 2016), while air quality remains persistently low (Akimoto 2003; Baldasano *et al.* 2003; Lelieveld *et al.* 2015; Cheng *et al.* 2016). Local declines in economically significant bee species have already been reported in certain regions of China (Teichroew *et al.* 2017). However, since air pollutants can travel not only between countries but also between continents, forming a global circuit (Uno *et al.* 2009; Lee *et al.* 2019), the expected pollinator crisis resulting from poor air quality should not be considered a localized issue. Furthermore, ongoing climate change is expected to increase the concentration of PM2.5. While the effects of climate change on PM2.5, and vice versa, may vary across regions, a substantial increase in PM2.5 mass concentrations is predicted in source regions and more populated areas (Fang et al. 2013; Silva et al. 2017). Additionally, a warming climate is expected to lead to more frequent and severe wildfires, which will contribute to increased PM2.5 emissions in many regions (Schuur et al. 2015; Liu et al. 2016; Wotton et al. 2017).

Despite the limited literature correlating worsening air quality with bee foraging or population decline, the interaction between air pollution and other potential stressors, as discussed earlier, can exacerbate this risk (Figure 2). This amplification arises from the increased likelihood of foragers encountering additional stressors such as insecticide residue and parasites during prolonged search for food and navigation between their nest and resources (Fuentes *et al.* 2016). Disorientation under a polluted sky can lead to extended foraging durations, similar to the disorientation experienced during natural atmospheric events like wildfire outbreaks. Prolonged foraging duration is a characteristic feature of disoriented honey bees (I'Anson Price *et al.* 2019). Considering that bees typically exhibit shorter foraging durations during the full bloom of floral resources, any trip longer than the average foraging trip duration can result in suboptimal foraging performance (Hemberger & Gratton 2018).

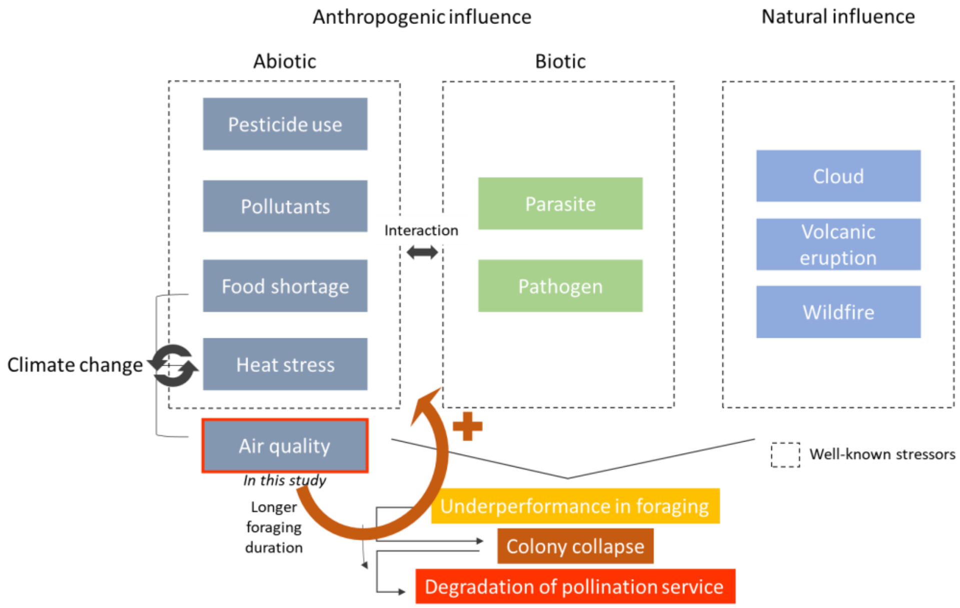

Figure 2. Demonstration of how air quality as an anthropogenic stressor can interact with pre-existing stressors. Underperformance of bees in foraging during poor air quality episodes as longer foraging trip duration increases chances for bee foragers of encountering other stressors. Poor air quality with a higher PM2.5 mass concentrations can act the same as natural stressors on underperformance of bees in foraging.

1.4 Research overview

1.4.1 Purpose of this study

This study aims to estimate the probable increase in the spatio-temporal magnitude of limited-visibility risk for honey bees (*Apis mellifera*) caused by a reduction in the DoLP due to increasing PM2.5 emissions. For this research purpose, three main sets of sub-studies were conducted, each primarily relying on field monitoring, ground observation, and future projection. Each of the first two studies has its own hypothesis and corresponding objective.

1.4.2 Research objectives and hypotheses

To assess the impacts of air quality on honey bee foraging performance, as indicated by foraging trip duration, which can also influence pollination efficiency, field-realistic colony monitoring was conducted (Objective 1). Considering that mean foraging trip durations have consistently been shown to be shorter than an hour in previous studies (Higginson *et al.* 2011; Perry *et al.* 2015; Colin *et al.* 2019; Okubo *et al.* 2020), it was hypothesized that an increase in foraging duration is strongly associated with ambient PM2.5 mass concentration. Additionally, it was hypothesized that honey bee foraging trip duration increases with an increase in the optical property of the atmosphere, known as the Depolarization Ratio (DR) (Hypothesis 1).

Furthermore, to quantitatively assess the relationship between air pollution levels and celestial DoLP and determine whether the increasing mass concentration of PM2.5 leads to a reduction in DoLP (Objective 2), a long-term ground-based observation of DoLP was conducted. Through this observation, an empirical relationship between ground-measured PM2.5 mass concentration and celestial DoLP was derived to predict the DoLP distribution across the sky, based on the dominant effect of PM2.5 on light scattering and atmospheric visibility (Hinds 1999; Liu *et al.* 2017; Zheng *et al.* 2017; Wang *et al.* 2019b; Dhaka *et al.* 2020; Won *et al.* 2020; Yao *et al.* 2021). In this dissertation, PM2.5 was a particular research interest as multiple scattering simulations have shown that changes in DoLP are most sensitive to fine-mode particles (Boesche *et al.* 2006; Chen *et al.* 2020). Here, a ground-based digital all-sky imaging system (ground-based imaging polarimetry) was employed, and the celestial DoLP was analyzed using cloud-free full-sky images collected between 2018 and 2019, as well as from 2020 to 2021. The polarization state of sunlight for each observation was expressed using Stokes parameters (Kreuter *et al.* 2010). The DoLP distribution across the sky was mapped, and an empirical relationship between PM2.5 and DoLP was parameterized.

This relationship was then applied to the air quality projection results using the global distribution of PM2.5, simulated by the ECHAM5/MESSy atmospheric climate chemistry model (EMAC), this model was chosen to evaluate the potential consequences of the absence of mitigation efforts for air quality. It assumes the continuation of national air pollution mitigation policies established in 2010, while considering anticipated population growth and economic development (Pozzer *et al.* 2012b; Lelieveld *et al.* 2015). “Risk hotspot” areas (an area of 1.1° by 1.1° in latitude and longitude) defined as where honey bees may experience limited visibility for at least one day in 2050 were estimated; this is critical to plant reproductivity, as even a one-day loss of pollination due to unsuccessful navigation of pollinators can have detrimental consequences (Ashman & J. Schoen 1994; Rader *et al.* 2013). Finally, the spatial extent of risk hotspots and the frequency of limited-visibility days (LVD) per hotspot (i.e., the number of LVD) were estimated at the global, regional, and national scales annually and seasonally. Further, increases in the extent of risk hotspots accompanied by increases in the frequency of LVD were estimated. The PM2.5 projection for 2010 from the same model as the base year data was used. Though the case of honey bee was investigated specifically since its polarotatic response on visual navigation is the most well-known, results of this study are possibly applied to other pollinator species. The structure of this dissertation is depicted in Figure 3.

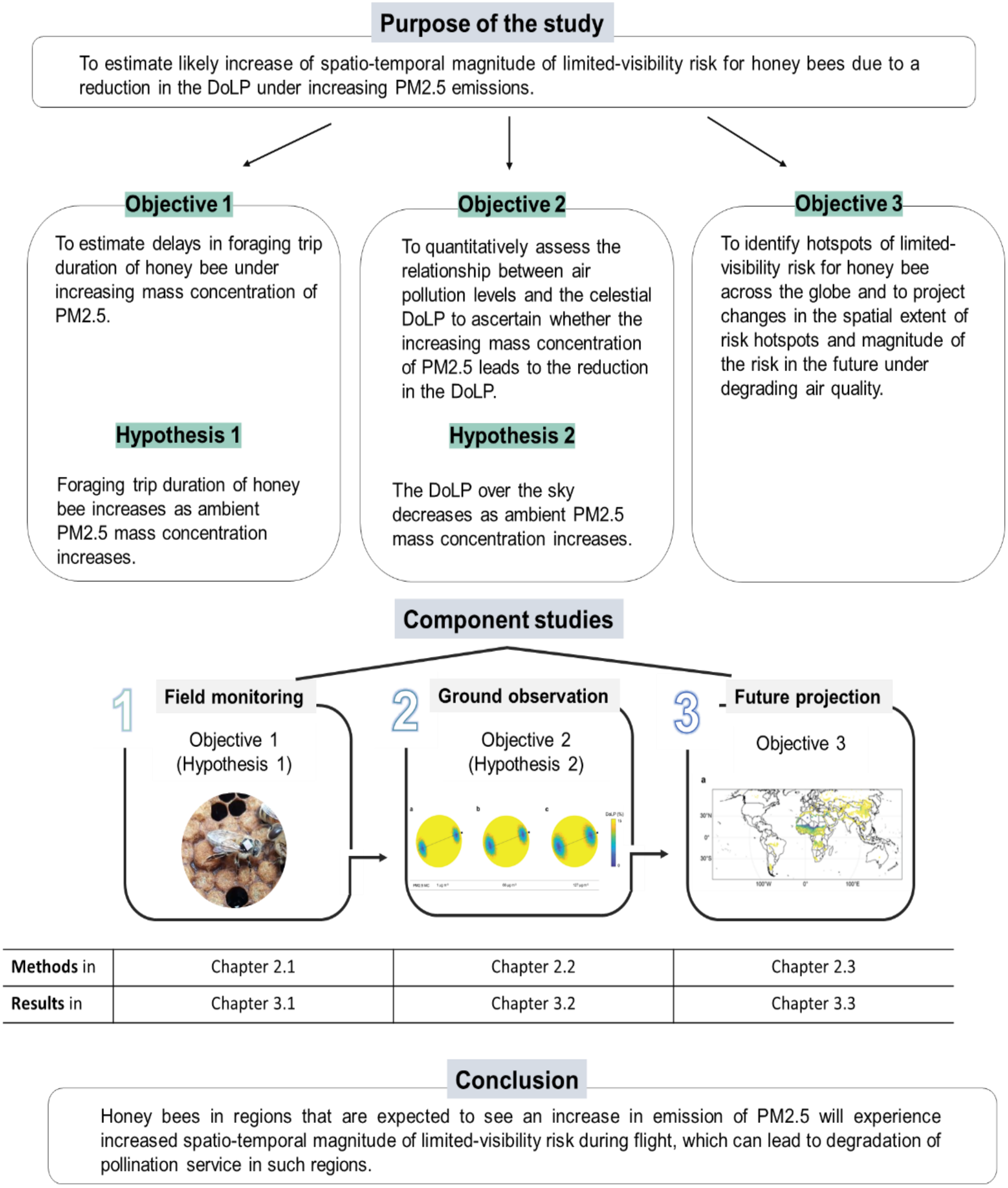

Figure 3. A structural diagram of this proposed study illustrating key elements-research hypotheses, objectives and expected conclusion. Chapter 3 presents the results corresponding to each research objectiv

2. Methodology

2.1 Colony monitoring with RFID

2.1.1 Study site

The experiment was conducted in an apiary on a hill bordering the Beijing Botanical Garden (BBG), Xiangshan park, Haidian District, Beijing, China (40° 0' 35" N, 116° 12' 2" E). The apiary is situated in close proximity to mountains, with the BBG within a 1 km radius. It is approximately 20 km northwest of the city center. The BBG is recognized as one of the largest ex-situ botanical gardens in Beijing, encompassing an area of 56 hectares and housing approximately 6,000 plant species. Throughout the study period, a variety of pollinator-dependent flowering species including *Malus spectabilis*, *Rosa chinensis*, *Iris sanguinea,* etc. were in full-bloom. The apiary is managed by the Institute of Apicultural Research, Chinese Academy of Agricultural Sciences. For the experiment, a colony comprising approximately 20,000 honey bees, with a single queen, was obtained from the apiary and housed in a standard Langstroth hive.

2.1.2 RFID tagging and colony monitoring

To monitor the foraging trip durations of worker bees, radio frequency identification (RFID) transponders (mic3® -TAG 16k, microsensys GmbH, Erfurt, Germany) were attached to the bees. The transponders had a square shape with dimensions of 2 x 1.7 x 0.5 mm and weighed less than 5 mg. A total of 400 worker bees of mixed ages were individually tagged with unique identification numbers (UIDs) stored in the RFID tags. At the entrance of the hive, a reader module (MAJA reader module 4.1) was installed to capture the UID and timestamp of each tagged bee as it passed by. The recorded timestamps were stored in a host computer. By comparing the recorded time points of the outbound and inbound trips, the duration of each foraging trip was calculated as the time difference between the two trips. For the analysis, only trip durations ranging from 10 minutes to 250 minutes were selected, excluding trips outside this range, which are considered either orientation flights or incomplete trips (Biesmeijer & Seeley 2005; Degen et al. 2015). Throughout the study period, a total of 74,104 observations (outbound-inbound trips) were recorded. However, due to overlapping timestamps caused by traffic at the hive entrance, only 181 "identifiable" pairs of foraging trips (equivalent to 362 timestamps) were included in the statistical analysis. The monitoring of foraging activities using the RFID system was conducted from April 27 to May 7, 2017.

2.1.3 Acquisition of optical property, ground-observed aerosol concentration and meteorological data

Optical property data

Although changes in PM2.5 mass concentration can explain the variation in the DoLP, the DoLP is the outcome of complex interactions between aerosol loading and the microphysical properties of aerosols, such as morphology, size, and refractive index (Chen *et al.* 2020). In order to examine the contribution of microphysical properties to DoLP variation, additional optical property data were utilized.

Optical property data that complied with our monitoring requirements were retrieved. The depolarization ratio (DR) at 532 nm, measured by Mie-scattering lidar in Beijing (39.977° N, 116.381° E), was adopted to investigate the effects of ambient aerosols on light polarization patterns.

The DR values measured between altitudes of 0.06 km and 0.72 km, which encompassed the lowest and highest altitudes common to the observation days, were averaged and used for analysis. DR serves as a reliable indicator of particulate matter irregularity (Pan *et al.* 2017), which is significant in terms of the degree of light polarization. A higher DR value (e.g., greater than 0.1) suggests the dominance of non-spherical particles in the atmosphere (Kim *et al.* 2010; Shimizu *et al.* 2016). As honey bees estimate distances and directions between their nest and floral resources during their outbound trips (Evangelista *et al.* 2014), values of the optical property variable (DR) and PM2.5 concentration measured at approximately the time when bees commenced foraging were used. However, since DR data were collected at quarter-hourly intervals and PM2.5 mass concentration data were collected hourly, data measured at the nearest time points to the outbound trips of the foragers were used. DR data were obtained from the Asian Dust and Aerosol Lidar Observation Network.

For the DoLP observations made using a ground-based imaging polarimetry system in Seoul, DR data that corresponded to the observations were obtained from the Korea Aerosol Lidar Observation Network. In addition, Extinction Coefficient (EC) data were also retrieved. EC provides a direct measure that can explain the variability in light extinction, which in turn affects the DoLP. This measure encompasses various microphysical and chemical properties of aerosols, such as size distribution, refractive index, and particle shape (Xie *et al.* 2008). To better understand EC, it is necessary to comprehend Aerosol Optical Depth (AOD), which represents the extinction of light and is the product of coefficients per unit mass of aerosols and the aerosol mass concentration. For instance, for sulfate aerosols, the optical depth is expressed as Equation (1).

$$AOD_{sulfate} = \alpha SO_4^{2-} m\ SO_4^{2-} H \qquad (1)$$

αSO_4^{2-} is the light-scattering mass efficiency of the aerosol, expressed in units of $m^2(g\ SO4^{2-})^{-1}$, $m\ SO_4^{2-}$ is the sulfate mass concentration (g m^{-3}), and H is the pathlength through the aerosol layer (m). The light-scattering mass efficiency is a quantity that, when multiplied by the mass concentration of sulfate, produces the sulfate aerosol scattering coefficient, b_{sp}. With a population of different types of aerosols in the atmosphere, not only b_{sp} but also b_{ep} (aerosol absorption coefficient) can be calculated. The EC is the sum of b_{sp} and b_{ep}.

In the global context, PM2.5 is predominantly classified into SNA (sum of sulfate, nitrate, and ammonium), OM (organic matter), BC (black carbon), dust and sea salt (Cheng *et al.* 2016). Each type of aerosol possesses different microphysical properties and refractive indices, which determine the extinction efficiency and subsequently influence the degree of light extinction (Dubovik *et al.* 2002). As stated earlier, light extinction, often represented by AOD, is the cumulative effect of two distinct modes: scattering and absorption. The impact of each mode on the DoLP may vary. Since the atmospheric aerosol column is typically composed of particles emitted from diverse sources, it is a mixture rather than a single aerosol type that prevails. Consequently, any model attempting to predict DoLP solely based on PM2.5 mass concentration cannot achieve a perfect fit, represented by R^2=1 or any other general regression model. Scattering-dominant aerosols encompass SNA and sea-salt particles, while absorbing aerosols, primarily BC, dominate at visible wavelengths (Li *et al.* 2022a).

In this context, single-scattering albedo (SSA), defined as the ratio of scattering coefficient (β_s) to total extinction coefficient (β_e) (Li *et al.* 2022a), serves as a useful parameter to assess the contribution of scattering to overall light attenuation. SSA is a comprehensive parameter that encapsulates essential information regarding the physical and chemical characteristics of aerosols (Pokhrel *et al.* 2016). Moreover, the absorption aerosol optical depth (AAOD) quantifies the contribution of absorbing aerosols to light extinction by applying the SSA (AAOD = AOD * (1-SSA)), as a decrease in SSA indicates a higher absorption by aerosols (Andrews *et al.* 2017). The global mean SSA at a wavelength of 550 nm (SSA550) over land is estimated to be 0.93 (Devi & Satheesh 2022). However, for most locations, very few AAOD or SSA retrievals are available after cloud-screening, as low-loading aerosols (AOD440 < 0.4 or AOD440 < 0.2 for AERONET Level 2 and Level 1.5 data, respectively) often introduce biases (Andrews *et al.* 2017; Mok *et al.* 2018). Unfortunately, the SSA440 (hereafter referred to as SSA) retrieval provided by AERONET (Level 1.5) exhibits a time difference of approximately 2 hours compared to our ground observation, as the earliest available SSA data throughout the day corresponds to a solar zenith angle (SZA) of approximately 76°, in contrast to the 90° SZA during our observation. AOD and SSA data were retrieved from the Aerosol Robotic Network (AERONET) operated by the National Aeronautics and Space Administration (NASA).

Ground-observed aerosol concentration

For PM2.5 mass concentrations in Beijing, the data were obtained from the Beijing Environmental Protection Monitoring Center. Ground-based DoLP observations were matched with near-real-time (maximum 15-minute intervals) PM2.5 mass concentration data obtained from the AirKorea network, operated by the Ministry of Environment (MOE). The monitoring station (37° 29' 53.3832´´, 126° 53' 24.1152´´) was located approximately 1 km from the polarimetry system. Site-specific atmospheric light extinction can vary due to different contributions from chemical components within PM2.5. Seoul is a suitable representation of anthropogenic PM2.5, particularly SNA (sulfate, nitrate, and ammonium) dominance found in many East Asian regions (Cheng *et al.* 2016).

To compensate for uncertainties in using SSA for DoLP estimation, another set of ground-measured data was examined. The mass concentrations of various components in PM2.5, such as SO_4^{2-}, NO_3^-, Cl^-, Na^+, NH_4^+, K^+, Mg^{2+}, Ca^{2+}, organic carbon (OC), elemental carbon (EC), S, K, Ca, Ti, V, Cr, Mn, Fe, Ni, Cu, Zn, As, Se, Br and Pb were measured at the Seoul Metropolitan Area Intensive Monitoring Site (SIMS) by the MOE between 2018 and 2021. These data were obtained in collaboration with the National Institute of Environmental Research. Although the SIMS was approximately 11 km away from our ground observation site, its location and data are considered representative of a wider region of Seoul (박종성 *et al.* 2015 in Korean). In general, during winter in Seoul, the contributions from SNA, OC, and EC are highest, with SNA (particularly nitrate) being the dominant component of PM2.5 (Park *et al.* 2018).

Meteorological variables

For colony monitoring in Beijing, daily meteorological data, including temperature (°C), humidity (%), wind speed (km/h), and cloud cover, were obtained for the study period. The data were retrieved online from CustomWeather, Inc. (timeanddate.com), specifically from the nearest time point to the outbound trip of foragers in the Xiangshan Park area, Beijing. Cloud cover was categorized into two levels: "non-overcast" and "overcast," as bees can still navigate as long as clear patches of sky are present.

2.2 Operation of ground-based imaging polarimetry system and estimation of DoLP over the sky

The DoLP across the full-sky hemisphere was observed using a ground-based imaging polarimetry system. The system utilized a commercial digital single-lens reflex camera equipped with a charge-coupled device (CCD). The ground-based full-sky imaging polarimetry system is uncomplicated yet ideal for mapping the celestial DoLP distribution (Kreuter *et al.* 2009; Foster *et al.* 2018). This system was composed of a camera (Nikon D70s), fish-eye lens (Lensbaby LLC, 5.8 mm, f/22, field-of-view ≈ 180), and linear polarizer filter (Cokin X160). The camera with the fish-eye lens was mounted on a tripod, positioned to ensure that the optical axis of the fish-eye lens was directed vertically towards the zenith. This method follows the system operation and image calibration described by Kreuter *et al*. (Kreuter *et al.* 2009). For a given sky, full-sky images were captured at four different polarizer angles (0°, 45°, 90°, and 135°), based on which three Stokes parameters, I, Q, and U, were calculated at each pixel using Equation (2); I is the light intensity, and $I(0°)$, $I(45°)$, $I(90°)$, and $I(135°)$ are the values at the polarizer angles of 0°, 45°, 90°, and 135°, respectively. The pixel-by-pixel (3008 × 2000 pixels) DoLP was then calculated using Equation (3). For visual presentation purposes, a color-coded map illustrating the DoLP distribution across the entire sky was generated using Matlab R2018b and ImageJ.

$$\begin{bmatrix} I \\ Q \\ U \end{bmatrix} = \begin{bmatrix} (I(0^{\circ}) + I(45^{\circ}) + I(90^{\circ}) + I(135^{\circ}))/2 \\ I(0^{\circ}) - I(90^{\circ}) \\ I(45^{\circ}) - I(135^{\circ}) \end{bmatrix} \tag{2}$$

- $I()$ = The intensity of radiation recorded in pixels when the linear polarization filter is at 0°, 45°, 90° and 135° from the camera top view.

$$DoLP = \frac{\sqrt{Q^2+U^2}}{I} \tag{3}$$

Only cloudless full-sky conditions were considered for the DoLP measurements, with a focus on capturing PM2.5-induced changes. Due to the strict sampling restrictions, a total of 40 samples were obtained over the four-year period (2018-2021). The ground-based imaging polarimetry observations were conducted at the predicted sunrise time to avoid any overexposure effects from the Sun. The DoLP theoretically reaches its maximum when the solar zenith angle (SZA) is 90°, such as during sunrise or sunset (Dahlberg *et al.* 2011). Additionally, the observations were limited to the period between the December solstice and the March equinox (December 21, 2018 - March 20, 2019, and December 21, 2020 - March 20, 2021) to minimize potential seasonal effects caused by the interaction of urban PM2.5, the planetary boundary layer, and relative humidity (RH) (Miao *et al.* 2019). RH variability can significantly impact the aerosol size distribution, chemical composition, and extinction characteristics through the hygroscopic growth of aerosols (Zheng *et al.* 2017). Moreover, water vapor directly influences light extinction, and RH often increases with height within the planetary boundary layer. For a given PM2.5 mass concentration, an increase in RH can result in higher light extinction (Zheng *et al.* 2017). Generally, the planetary boundary layer height (PBLH) and RH are lowest during winter compared to other seasons (Wang *et al.* 2019a). Although the lowest PBLH during winter can enhance mixing, the low rate of hygroscopic growth of particles may offset this effect (Zheng *et al.* 2017).

Initially, our ground observations were conducted at both sunrise and sunset. However, the sunset observations from our analysis were excluded due to the significant effects of relative humidity (RH) and moonlight on the DoLP during sunset hours. Here, the observational data obtained from both sunrise and sunset is present to demonstrate the potential effects of RH on DoLP. The DoLP observations were classified into three groups: 1) all (sunrise + sunset, N=68), 2) sunrise only (N=40), and 3) sunset only (N=28) datasets, and conducted statistical tests for each dataset. It is important to note that the sunset dataset had a relatively smaller sample size compared to the other two datasets. The PM2.5-DoLP relationship was found to be significant ($p<0.001$) for all datasets. To investigate whether RH had a minimal influence on DoLP variation, the correlation between PM2.5 and DoLP was tested while considering the variation in RH. Two different scenarios were examined: first, the relationship between PM2.5 mass concentration and DoLP while controlling for the correlation of RH with both variables (partial correlation test), and second, the relationship between PM2.5 mass concentration and DoLP while accounting for the effects of RH on DoLP only (semi-partial correlation test). The results are summarized in Table 1 (a-b). In all three datasets, both for average and maximum DoLP, the correlations between PM2.5 and DoLP were statistically significant, indicating a strong association between PM2.5 and DoLP even without considering the potential effects of RH on both variables.

Furthermore, in addition to the impact of RH on light extinction through the hygroscopic growth of particles, water vapor directly affects light extinction. Therefore, the same correlation tests were conducted to examine the RH-DoLP relationship while considering the potential effects of PM2.5 levels. The relationship was only statistically significant in the All dataset, demonstrating that increasing RH leads to a decrease in DoLP (Table 1 (c-d)). However, the zero-order correlations between PM2.5 mass concentration and the average and maximum DoLP in the Sunrise dataset, as observed in our original analysis, remained statistically significant. These high correlations (r=-0.75 and -0.81 for average and maximum DoLP, respectively) suggest that RH has a minimal influence on controlling the PM2.5-DoLP relationship. The RH values recorded during our ground-based observations ranged from 22% to 88%.

Table 1. Results from the partial and semi-partial correlation analyses examining the relationships between PM2.5 mass concentration, RH, and DoLP in different datasets. Bold text indicates statistically significant differences with a *p*-value<0.01.

a) Correlation test results for PM2.5 mass concentration and the average DoLP.

Dataset	All		Sunrise		Sunset	
Test	*r*	*P*-value	*r*	*P*-value	*r*	*P*-value
Partial correlation	**-0.44**	**<0.01**	**-0.66**	**<0.01**	**-0.58**	**<0.01**
Semi-partial correlation	**-0.40**	**<0.01**	**-0.54**	**<0.01**	**-0.48**	**<0.01**

b) Correlation test results for PM2.5 mass concentration and the maximum DoLP

Dataset	All		Sunrise		Sunset	
Test	*r*	*P*-value	*r*	*P*-value	*r*	*P*-value
Partial correlation	**-0.64**	**<0.01**	**-0.76**	**<0.01**	**-0.62**	**<0.01**
Semi-partial correlation	**-0.57**	**<0.01**	**-0.61**	**<0.01**	**-0.52**	**<0.01**

c) Correlation test results for RH and the average DoLP

Dataset	All		Sunrise		Sunset	
Test	*r*	*P*-value	*r*	*P*-value	*r*	*P*-value
Partial correlation	**-0.35**	**<0.005**	-0.05	0.74	0.3	0.13
Semi-partial correlation	**-0.31**	**<0.01**	-0.04	0.79	0.25	0.21

d) Correlation test results for RH and the maximum DoLP

All			Sunrise		Sunset	
Test	*r*	*P*-value	*r*	*P*-value	*r*	*P*-value
Partial correlation	-0.02	>0.1	0.02	0.89	0.27	0.17
Semi-partial correlation	-0.02	>0.1	0.02	0.91	0.23	0.25

The ground-based imaging polarimetry system mapped the distribution of DoLP over multiple wavelength bands. However, only the DoLP of the blue band in the visible spectrum was considered in this study. The camera's blue sensor has a spectral response that peaks at 450 nm. Although honey bees are most sensitive to polarized skylight in the ultraviolet (UV) spectrum (345-360 nm) (Barta & Horváth 2004; Sakura *et al.* 2012; Ogawa *et al.* 2017), there is only a slight qualitative difference between the DoLP values obtained from the blue band and the UV band (Pomozi *et al.* 2001). The DoLP of the UV band can be significantly smaller than that of the blue band, both under clear and polluted skies (Brines & Gould 1982; Coulson 1988; Dahlberg *et al.* 2011). It is worth noting that bumblebees (*Bombus hortorum*), another widespread bee pollinator, are most sensitive to polarized skylight in the UV (353 nm) and blue (430 nm) spectral regions (Barta & Horváth 2004). Additionally, since the DoLP exhibits greater sensitivity for smaller solar zenith angles (SZA) and longer wavelengths (Pust & Shaw 2012; Shaw *et al.* 2014), measuring the DoLP in the blue band at sunrise is reasonable for increased accuracy.

The results of exponential regression analysis showed a significant relationship between EC and DoLP, indicating that both the average and maximum DoLP values decreased as EC increased ($p < 0.01$). However, the adjusted R2 values, for example, 0.25 for the EC-maximum DoLP relationship, were much lower than those of the relationships between PM2.5 mass concentration and DoLP (adjusted R^2=0.72, P<0.01). PM2.5 mass concentration was found to be correlated with EC (adjusted R^2= 0.42, P<0.001). This suggests that the mass concentration of small particles with diameters less than 2.5 μm (as the growth of even smaller particles to optically more active sizes generally falls within this range) was a useful variable in explaining the changes in DoLP.

The near-real-time (15 min-interval at maximum) ground-measured PM2.5 at the time of the ground-based imaging polarimetry system operation each day was retrieved from the AirKorea network. The monitoring station (37° 29' 53.3832″, 126° 53' 24.1152″) was located approximately 1 km from the polarimetry system.

2.3 Statistical modelling of the empirical PM2.5 mass concentration-DoLP relationship for future projection

2.3.1 Threshold concentration of PM2.5 for the lower-bound (LB) and upper-bound (UB) estimations

A non-linear square (NLS) regression model (Equation 4) with a Gauss–Newton algorithm was constructed to derive an empirical relationship between PM2.5 mass concentration and DoLP. In this study, the NLS regression model showed a better fit than the linear regression model (ΔAkaike Information Criterion = 259.41).

$$\ln(Y_{\mathrm{obs}}) = \hat{}\beta0 + \hat{}\beta1X + e \qquad (4)$$

Y_{obs} : Observed DoLP (%)

X : PM2.5 ($\mu g\ m^{-3}$)

$\hat{}\beta0$, $\hat{}\beta1$: Fitted coefficients

e : Residual error

To reduce the uncertainty arising from the small sample size (N=40), bootstrap simulations were performed 2,000 times based on the NLS equation.

As previously discussed, the perceptual threshold of DoLP for honey bees is 10%, which indicates that honey bees do not perceive a DoLP of less than 10%. However, for achieving a perfect orientation, a DoLP of 15% or more should be exhibited over the sky to bees during flight (Brines & Gould 1982; Rossel & Wehner 1984; Henze & Labhart 2007; Von Frisch 2013). Therefore, a DoLP of 15% was defined as the navigational threshold in this study. The DoLP is symmetrically distributed over the sky (Hegedüs *et al.* 2007b), and is close to zero near the Sun and the maximum at a right angle to the Sun (Hegedüs *et al.* 2007b, a; Hegedüs *et al.* 2007c). Honey bees determine their orientation by inferring the direction in which a band of the maximum DoLP occurs over the full-sky (Rossel & Wehner 1984). However, complete visibility of the sky containing the band of maximum DoLP is not always guaranteed; this is often the case under thick canopies and clouds, that honey bees are more likely to encounter. In fact, as long as the DoLP is above the navigational threshold, honey bees can use the radiative information even from a very tiny patch in "any part" of the full sky (a minimum of 10° of the so-called "celestial window") (Rossel & Wehner 1984; Rossel 1993; Labhart 1996). Therefore, the best-fit PM2.5 mass concentrations corresponding to the threshold DoLP from average DoLP and maximum DoLP over the sky for LB and UB estimations, respectively, was used. The best-fit PM2.5 mass concentrations from the regression models, corresponding to the average and maximum DoLPs, as threshold values for the LB and UB estimations, respectively, was applied. These PM2.5 mass concentration thresholds were the best-fit estimates within confidence intervals (CIs) from the NLS regression model for each PM2.5 mass concentration–average DoLP and PM2.5 mass concentration–maximum DoLP relationship. Then these PM2.5 mass concentrations were applied on air quality projections for 2050.

2.3.2 Applying the PM2.5 mass concentration-DoLP relationship on air quality projection

The ECHAM5/MESSy atmospheric chemistry (EMAC) general circulation model with a spatial resolution of spherical spectral truncation of T106 was used, which corresponds to a quadratic Gaussian grid of approximately 1.1° by 1.1° in latitude and longitude. The EMAC comprises submodels describing the low-level Earth systems to tropospheric and stratospheric processes and allows the simulation of the feedback of air pollution. The global distribution of PM2.5 for the year 2010, simulated by EMAC, agreed with the observational data (Lelieveld *et al.* 2015). This model was chosen to evaluate the potential consequences of the absence of mitigation efforts for air quality. It assumes the continuation of national air pollution mitigation policies established in 2010, while considering anticipated population growth and economic development, which represented a feasible future (Pozzer *et al.* 2012b; Lelieveld *et al.* 2015). Since it is challenging to fully account for regional disparities in effects of climate change in future air quality the future air quality simulations, the scenario adopted in this study are based on the average climatology of the period 2000-2009.

In detail, the scenario here is different from the Representative Concentration Pathways 8.5, in that the former did not consider possible effects of climate change on PM2.5 emissions (Pozzer *et al.* 2012b). Though the effects of climate change were not reflected in the air quality projection, the model accounted for population growth and economic development (Lelieveld *et al.* 2015). The model was based on projections for energy and fuel use and land-use related projections computed by the Prospective Outlook for the Long-term Energy System (POLES) model and the Integrated Model to Assess the Global Environment (IMAGE) (Pozzer *et al.* 2012b). The POLES model is a global sectoral simulation model for the development of energy scenarios until 2050.

While a range of emission scenarios is available, this particular scenario was chosen for two main reasons. Firstly, although the model does not consider the effects of climate change, it incorporates population growth and economic development. Consequently, regions that have transitioned from manufacturing to service-based industries, i.e., developed countries, did not show increases in the number of limited visibility days. While stringent clean-air policies have improved air quality in some regions, it is uncertain whether such environmental regulations can override socioeconomic strategies. China's air quality started improving before 2010, to some extent reflecting this trend. Additionally, it is challenging to foresee the diverse pathways for future policy implementation (Chowdhury *et al.* 2018). Secondly, the objective was to emphasize the consequences of inadequate actions. Despite the possibility of technological advancements reducing emissions in the future (Lelieveld *et al.* 2015), the aim was to illustrate the outcomes "without such actions." Therefore, countries that have witnessed improvements in air quality, such as China, should intensify their efforts, while others should be more alert. Consequently, numerous studies examining future mortality rates associated with deteriorating air quality (Lelieveld *et al.* 2013; Lelieveld *et al.* 2015; Chowdhury *et al.* 2022) consider this scenario as representing a feasible future and utilize the air quality projection based on this scenario.

Of additional note is that this global ECHAM5/MESSy atmospheric chemistry-general circulation model is the only hour-based global air quality projection model. With this advantage, it was possible to single out projection results of a specific time window (8:00-16:00 after the time zones of each pixel converted to local time, please refer to Methods) at which honey bees actively forage. More detailed information on the projection of PM2.5 by the EMAC simulations can be found in Lelieveld et al. (Lelieveld *et al.* 2015) and Pozzer et al. (Pozzer *et al.* 2012a).

The simulated PM2.5 results were analyzed by season (i.e., MAM, JJA, SON, and DJF). The projection results for December, January, and February within the same year (2050 or 2010) were grouped. Land covers that are outside the scope of this study (land covers labeled as barren or sparsely vegetated, ocean, snow, and ice) were filtered out using the Global Land Surface Data Assimilation System (GLDAS) NOAH version 3.6, based on MODIS (Moderate Resolution Imaging Spectroradiometer) IGBP (the International Geosphere-Biosphere Programme) Vegetation Type classification (Rodell *et al.* 2004).

In this study, at least one occasion of limited visibility during the day was defined as a limited-visibility day; this is relevant to the energetics of honey bees and their interactions with plants. Many pollinator-dependent flowers bloom only for short durations of a few days (albeit for a few months in the tropics) (Heinrich & systematics 1975). Some flowers have even more limited lifetimes that are as short as one day or a few hours per day, during which optimal pollination should be provided (Rader *et al.* 2013). Honey bees conform their foraging to energetics (Heinrich & systematics 1975). As individual worker honey bees can only undertake a limited number of foraging trips in their lifetime, they maximize their foraging efficiency (Kacelnik *et al.* 1986). Thus, honey bees avoid undertaking foraging trips with a duration longer than the time expected to be sufficient for pollination, since a longer foraging trip duration means greater energy expenditure (Kacelnik *et al.* 1986). This eventually reduces the opportunity for plants to receive optimal pollination services. Considering the diurnal fluctuations of nectar availability from flowers and radiative information from the Sun, the estimation time slot was limited to between 8:00 and 16:00. This time slot is reasonable upon accounting for the regional and seasonal variations in sunrise-sunset times.

2.3 Data analysis

All statistical analyses were performed using R version 3. 2. 5 (Team 2016). The Tukey Honest Significant Differences test (ANOVA Tukey multiple comparisons) was also conducted the R function *TukeyHSD* to compare group differences of mean foraging trip durations during the pre-dust storm, dust storm, and post-dust storm periods. Due to a maintenance issue, it was possible to collect data for May 2, so this date was omitted in the pre-dust storm period. Average foraging trip duration for each period and *P*-values of the ANOVA Tukey multiple comparisons were calculated through 10,000 parametric bootstrap replicates.

The effect of the predictor variables (DR, PM2.5 mass concentration and meteorological variables) on foraging trip duration of honey bee was determined using a generalized linear model (GLM). The GLM with Gamma family (link = log) was fitted using the R function *glm() in* package *lme4*. To eliminate possible impacts of the dust storm event on foragers' fitness and to evaluate pure effects of air quality on foraging performance, data obtained during post-storm period were excluded in the model (N = 138). Predicted probabilities on foraging trip duration from the model against one of the independent variables (IVs) for a given value of other IVs were calculated using package *TeachingDemos*. Interaction effects of PM2.5 mass concentration and overcast sky on the foraging duration are plotted using package *interactions*. Different models were evaluated using Akaike's criteria using package *bbmle*. Multicollinearity between predictor variables was assessed by the variance inflation factor (VIF) using the R function *vif()* in package *car*

Parameterization of PM2.5 mass concentration-DoLP relationship and analyses of global data were conducted using the packages "ncdf4" and "dplyr". Time zone conversion was conducted using the packages “sf”, “lutz,” “purrr”, “lubridate,” and “googleway” Google Maps API package. Data visualization (mapping) was conducted using the packages “sp”, “maps”, “rgeos”, “maptools”, “rworldmap”, “ggplot2”, “ggalt”, and “ggthemes”.

3. Quantitative analyses of the underperformance of honey bee in visual navigation under degrading air quality

3.1 Foraging trip duration of honey bee under different levels of air quality

Results from the field monitoring of a hive revealed that honey bee foragers spent approximately 71% more time on heavily polluted days compared to their previous average foraging duration. Interestingly, even after the dust storm had passed, the bees continued to invest 71% more time (on average) in foraging compared to before the dust storm (Figure 4). On May 4th, when the hourly PM2.5 mass concentration reached its maximum, the daily average foraging duration was approximately 77 minutes, which was about 32 minutes longer than the daily average prior to the dust storm. The comparison between the average foraging durations on the dust storm day and the post-dust storm days did not show a significant difference (Table 2). However, both the average foraging durations during and after the dust storm were significantly greater than the pre-dust storm levels (P<0.05 and P<0.001, respectively).

Using a GLM, the effects of the depolarization ratio (DR) and PM2.5 mass concentration on each foraging trip recorded from April 27 (pre-dust storm period) to May 4 (dust storm period) were assed (Table 3). The GLM model included real-time DR, PM2.5 mass concentration, meteorological variables (including cloud cover), as predictor variables. The selection of the best GLM model was based on evaluation using Akaike's criteria (Table 4). No multicollinearity was found among the predictor variables (Table 5).

These results indicate a strong association between DR, PM2.5 mass concentrations, and foraging duration (P=0.042 and P<0.001, respectively). As DR increases, foraging duration decreases, suggesting that when the atmosphere is dominated by more spherical urban pollutants (smaller DR) than mineral dust (larger DR), bees are predicted to spend more time foraging. Higher PM2.5 mass concentrations are associated with delays in foraging. Regardless of DR, foraging trip duration increases with increasing PM2.5 mass concentration, considering the other predictors at constant values (Figure 5). When foraging trip duration was regressed on DR only (alongside meteorological variables) in our study, DR did not show any significant effect, while the opposite was observed for the PM2.5 mass concentration (Table 6). Although cloud cover as a single predictor did not significantly impact honey bee foraging duration, a pronounced effect of PM2.5 mass concentration was observed under overcast sky conditions (P=0.036, Figure 6). Meteorological factors were not found to be associated with the time spent foraging by bees.

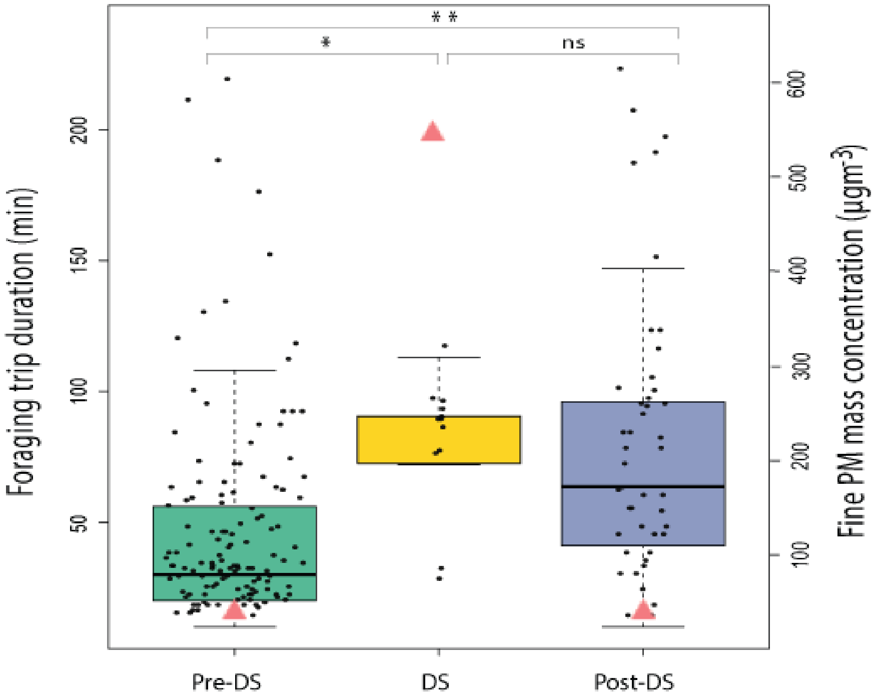

Figure 4. Foraging duration (min) of honey bee foraging trips (*N*=181) during pre-dust storm (Pre-DS, April 27 – May 3), dust storm (DS, May 4), and post-dust storm (Post-DS, May 5 - 7) period. Daily foraging duration was resampled 10,000 times. Note that only a few observations (*N*=12) were available during DS. ▲ indicates then mean fine PM (PM2.5) mass concentration of Pre-DS (48 μg m^{-3}), DS (573 μg m^{-3}), and Post-DS (49 μg m^{-3}) period. Hourly PM2.5 mass concentrations between the earliest and latest foraging activity recorded of each day were averaged. * and ** denote significance as P<0.05 and P<0.001, respectively, by ANOVA Tukey multiple comparisons of means 95% family-wise confidence level. ns: not significant (Table 2).

Table 2. Average foraging trip duration significantly increased on the day of DS outbreak and was not recovered to the pre-DS level even after the event had ceased. (A) Average foraging trip duration (min) of individual foragers (N=181) between April 27 – May 7. (B) ANOVA Tukey multiple comparisons of means 95% family-wise confidence level (after Fligner-Killeen's test). * and ** indicate P<0.05 and P<0.001, respectively. Daily foraging durations were resampled 10,000 times.

A

Average Foraging Duration (mins)	Pre-DS	DS	Post-DS
	45.04±11.30	76.74±7.18	76.55±15.39

B

Group	Difference	Lower value	Upper value	*P* value
Pre-DS/DS	-31.56	-61.85	-1.26	**<0.05***
Pre-DS/Post-DS	-31.20	-48.47	-13.93	**<0.001****
Post-DS/DS	-0.36	-32.86	32.15	**0.1**

Table 3. Effects of predictor variables (optical property (DR) and PM2.5 mass concentration, and meteorological variables) on foraging trip duration of individual foragers. * and ** indicate P<0.05 and P<0.001, respectively.

	Estimate	Std.Error	t-value	*P* value
(Intercept)	3.111	0.973	3.196	**0.002***
DR	-4.457	2.165	-2.059	**0.042***
PM2.5 mass concentration	0.004	0.001	4.112	**<0.001****
Cloud cover (non-overcast)	0.574	0.393	1.458	0.147
Temperature	0.040	0.027	1.516	0.132
Wind speed	0.007	0.034	0.213	0.832
Humidity	-0.003	0.010	-0.281	0.779
PM2.5 mass concentration: Cloud cover	-0.027	0.013	-2.115	**0.036***

Table 4. Different models were evaluated using Akaike's criteria. The best-fitting model with lower Akaike information criterion (AIC) is in bold.

Model (GLM, family=Gamma, Link=log)	*ΔAIC*	*df*	*Δ AIC weight*	*Residual deviance*
FD ~ DR + PM2.5 * C + T + W + H	**0.0**	**9**	**0.469**	**59.655**
FD ~ DR * PM2.5 + C + T + W + H	5.3	9	0.034	61.814
FD ~ PM2.5 + C + T + W + H	6.0	7	0.023	63.828
FD ~ DR * PM2.5 * C + T + W + H	3.5	12	0.081	58.661
FD ~ DR + PM2.5 + C + T + W + H	3.3	8	0.092	61.815
FD ~ DR + C + T + W + H	15.6	7	<0.021	68.073
FD ~ PM2.5 + DR * C + T + W + H	1.6	9	0.210	60.307
FD ~ PM2.5 * C + T + W + H	3.3	8	0.091	61.827

- Model structure (the best model as an example):

  $\ln(FD) = \hat{}\beta_0 + \hat{}\beta_1 X_1(DR) + \beta_1 X_2(PM2.5)* \beta_3 X_3(C) + \beta_4 X_4(T) + \beta_5 X_5(W) + \beta_6 X_6(H) + e$

  * indicates interaction terms

- Abbreviations:

  FD: Foraging duration (min)

  PM2.5: PM2.5 mass concentration ($\mu g\ m^{-3}$)

  DR: Depolarization ratio

C: Cloud-cover

T: Temperature

W: Wind speed

H: Humidity

Table 5. Detecting multicollinearity between predictor variables of different models based on VIF. VIF smaller than 10 suggests the model does not have a collinearity issue (Naimi & Araújo 2016)**.**

Model	Predictor variable						
(Best model) FD ~ DR + PM2.5 * C + T+ W + H	**PM2.5**	**DR**	**C**	**T**	**W**	**H**	**PM2.5 *C**
	3.59	**5.61**	**6.79**	**2.79**	**1.83**	**3.67**	**3.94**
FD ~ PM2.5 + DR * C + T + W+ H	PM2.5	DR	C	T	W	H	DR*C
	3.69	6.21	39.46	2.43	1.73	3.86	35.42
FD ~ DR * PM2.5 + C + T + W + H	PM2.5	DR	C	T	W	H	DR*PM2.5
	117.48	6.66	3.10	2.61	1.53	5.60	137.71

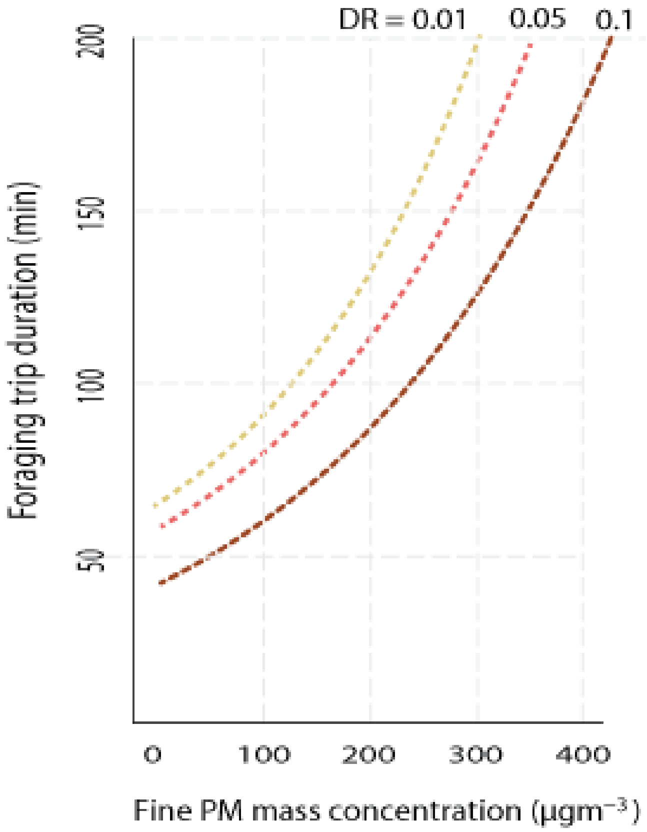

Figure 5. Predicted foraging trip duration (min) from the model against PM2.5 mass concentration for given values of the other predictors. Temperature = 28 ℃, Wind speed = 7 km h^{-1}, Humidity = 10%, Cloud-cover = Overcast.

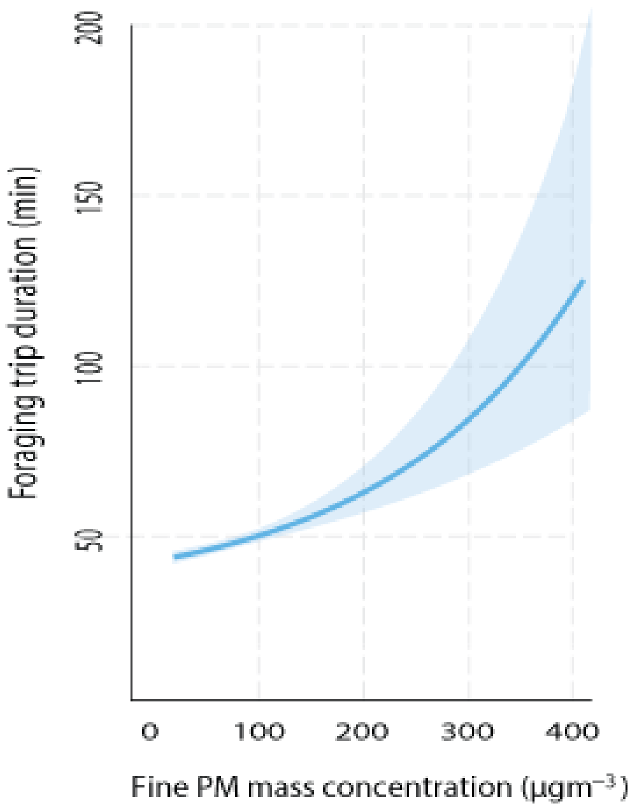

Figure 6. Predicted effects on PM2.5 mass concentration on foraging trip duration under overcast skies. All the other predictor variables are mean-centered. The solid line indicates the mean slope estimate, and the shaded area is the predicted 95% confidence interval.

Table 6. Effects of each DR, PM2.5 mass concentration, and cloud cover on foraging trip duration alongside meteorological variables evaluated by GLMs (family = Gamma, log = link). * and ** indicate *p*<0.05 and *p*<0.001, respectively.

1) Model: FD ~ DR + T + W + H (ΔAIC : 13.9)

	Estimate	**Std.Error**	**t-value**	***P* value**
(Intercept)	3.223	0.756	4.264	**<0.001****
DR	1.085	1.117	0.972	0.333
T	0.002	0.023	0.087	0.931
W	0.064	0.031	2.087	**0.039***
H	0.002	0.007	0.262	0.794

2) Model: FD ~ PM2.5 + T + W + H *(*ΔAIC : 6.1)

	Estimate	**Std.Error**	**t-value**	***P* value**
(Intercept)	2.849	0.665	4.287	**<0.001****
PM2.5	0.001	0.0005	2.502	**0.014***
T	0.021	0.023	0.918	0.360
W	0.050	0.030	1.657	0.100
H	0.002	0.007	0.298	0.766

3) Model: FD ~ C + T + W + H (ΔAIC : 15.1)

	Estimate	**Std.Error**	**t-value**	***p* value**
(Intercept)	3.755	0.624	6.017	**<0.001****
C	-0.088	0.192	-0.455	0.650
T	-0.010	0.021	-0.474	0.637
W	0.071	0.032	2.195	**0.030***
H	-0.002	0.007	-0.292	0.770

3.2 Relationship between PM2.5 mass concentration and DoLP of skylight

Based on ground-based imaging polarimetry, the association between the DoLP over the sky and ground-measured PM2.5 mass concentration was investigated. Figure 7 displays full-sky images representing different DoLP distributions over a cloud-free sky corresponding to the lowest PM2.5 mass concentration (1 μg m^{-3}, Figure 7a), the estimated average of the maximum and minimum PM2.5 mass concentration (66 μg m^{-3}, Figure 7b), and the highest PM2.5 mass concentration (127 μg m^{-3}, Figure 7c) among the 40 observation samples. The DoLP distribution exhibited axial symmetry along the solar-antisolar meridian, with the lowest DoLP near the Sun and the highest around the zenith (90° from the Sun). As the PM2.5 mass concentration increased, the sky region with DoLP below the navigational threshold (15%) expanded, indicating a reduction in the areas of the sky containing polarized light cues essential for honey bee navigation (Figure 8).

To establish an empirical relationship between PM2.5 mass concentration and the DoLP distribution over the sky, NLS regression models were constructed based on our observational data. For future estimations, the average and maximum DoLPs over the sky for each observation were utilized to determine the likely range of PM2.5 mass concentration corresponding to the navigational threshold (refer to Chapter 2, Methodology section for further details). The observed average (Figure 9a) and maximum DoLPs (Figure 9b) demonstrated a decrease with increasing PM2.5 mass concentration ($P<0.001$ for both average and maximum DoLPs). The model underwent 2,000 bootstrapping iterations to estimate the uncertainty in the observed data distribution. The model estimated the lower and upper bound PM2.5 mass concentrations matching the navigational threshold from the average and maximum DoLPs as 130 μg m^{-3} (CI: 110-160 μg m^{-3}) and 240 μg m^{-3} (CI: 206-292 μg m^{-3}), respectively. Thus, when atmospheric PM2.5 mass concentrations surpass these threshold values, honey bees are likely to encounter impaired navigation. The estimations with PM2.5 mass concentrations of 130 μg m^{-3} and 240 μg m^{-3} applied as threshold concentrations are referred to as the LB (lower bound) and UB (upper bound) estimations, respectively.

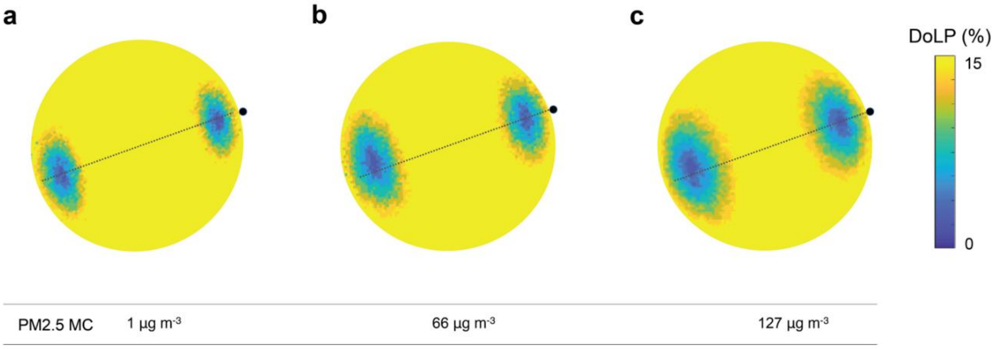

Figure 7. Full-sky images of the DoLP distribution depending on PM2.5 mass concentration. The navigational threshold of DoLP for honey bees (15%) is used as the maximum boundary of the DoLP range. Depending on PM2.5 mass concentration, the observed DoLP (average and maximum values) and observation date are as follows: a. 1 μg m^{-3}, DoLP (24.33% and 52.8%), December 29, 2018; b. 66 μg m^{-3}, DoLP (19.83% and 36.6%), January 23, 2019; and c. 127 μg m^{-3}, DoLP (17.3% and 33.12%), January 15, 2019. The approximate position of the Sun and solar-antisolar meridian are indicated as a black dot and dashed line, respectively, in each image. MC stands for mass concentration.

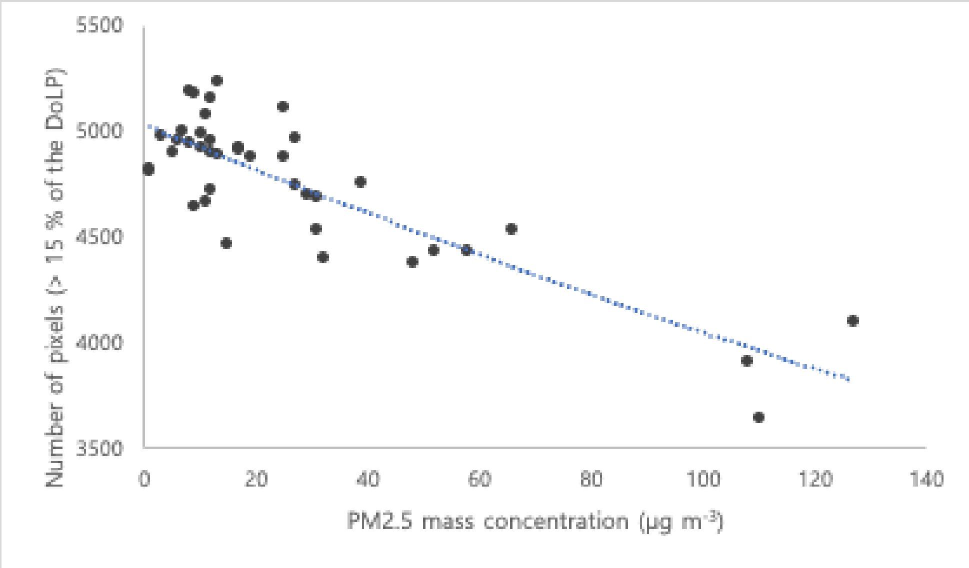

Figure 8. A statistically significant relationship between the PM2.5 mass concentration and the total size of the full-sky region including the DoLP greater than the threshold. The size exponentially decreased as the PM mass concentration increased. Since this analysis is based on photographic images, the size is represented by the number of pixels, each of which possesses the DoLP greater than 15%. *F*-statistic: 99.32, P<0.001 ($y = 5029.5e^{-0.002x}$, Adjusted R^2=0.716).

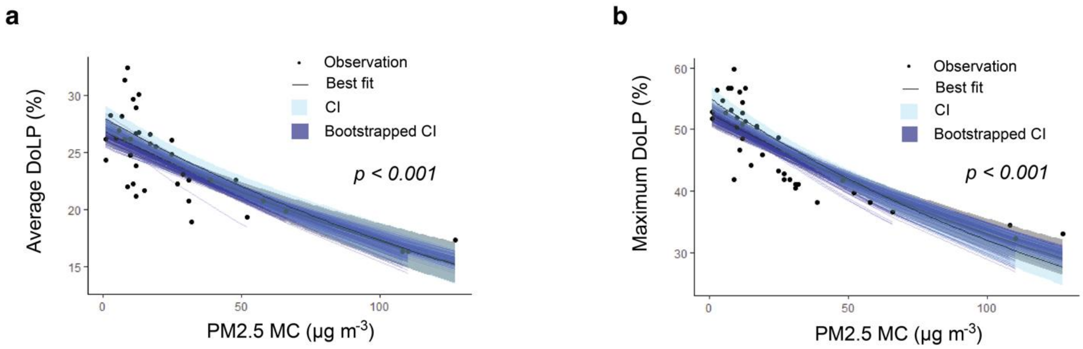

Figure 9. Statistical relationship between PM2.5 and the DoLP distribution over the sky. a: Relationship between PM2.5 mass concentration and the average DoLP over the sky. b: Relationship between PM2.5 mass concentration and the maximum DoLP over the sky. Observational sample points from the ground-based imaging polarimetry and a fitted line from the NLS regression are indicated as black dots and solid black lines, respectively. The 95% CI and the bootstrapped 95% CI are shown. MC stands for mass concentration.

To assess the model's performance, a comparison between the model's predictions and ground-based DoLP observation data collected in Beijing was conducted, utilizing a multi-wavelength sun photometer (unpublished data, obtained with the assistance of Dr. Cheng Chen from the Generalized Retrieval of Atmosphere and Surface Properties, France). It should be noted that these observations were only conducted sporadically (Figure 10 and Table 7). The observed maximum DoLPs in Beijing, corresponding to PM2.5 mass concentrations of 292 μg m^{-3} and 343 μg m^{-3} (on February 22, 2011, at 11:00 and 12:00, respectively), were 7% and 6%, respectively. In contrast, our model estimated confidence intervals (CIs) for each mass concentration as 10-17% and 7-14%, respectively. Even in the absence of such extreme haze events, the observed maximum DoLPs were 32% and 25% for PM2.5 mass concentrations of 75 μg m^{-3} and 100 μg m^{-3}, respectively. Our model predicted CIs for each mass concentration as 35-39% and 30-35%.

It is worth noting that the observed DoLPs in Beijing were slightly below the CIs predicted by our model. This discrepancy can be attributed to the difference in observation timings. In Beijing, the observations were conducted at 11 AM and 12 PM, whereas in our study, observations were limited to sunrise when the DoLP is expected to be at its maximum throughout the day.

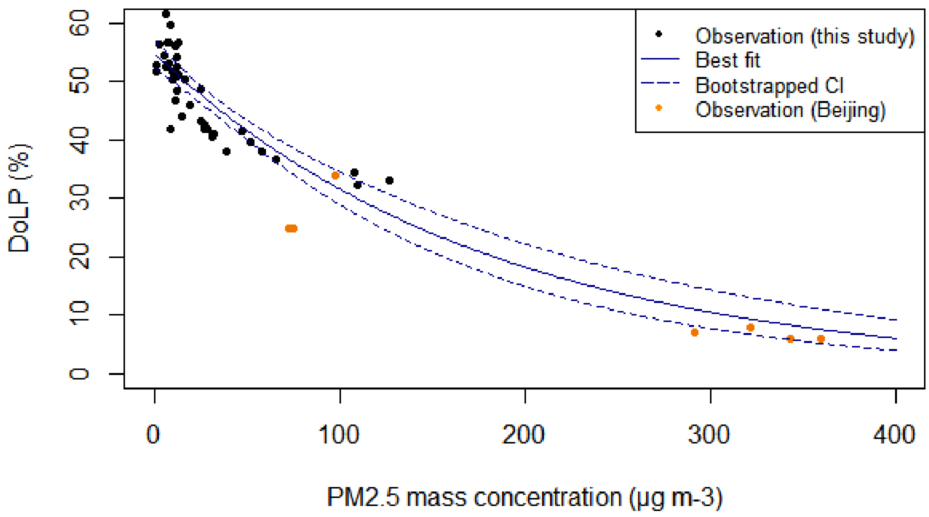

Figure 10. PM2.5 mass concentration-DoLP model in this study with DoLP observation data collected in Beijing included.

Table 7. Additional information on the observation data collected in Beijing. PM2.5 mass concentration and DoLP data were provided by Dr Cheng Chen at the Generalized Retrieval of Atmosphere and Surface Properties, France. AOD, AAOD and SSA (Level 1.5) measured at 440 nm were retrieved from AERONET. AOD: Aerosol Optical Depth, AAOD: Absorption Aerosol Optical Depth, SSA: Single-Scattering Albedo.

Date	Local time	PM 2.5 mass concentration (µg m^{-3})	DoLP	AOD	AAOD	SSA
Feb 22, 2011	11:00	292	7	3.1	0.24	0.927
	12:00	343	6	2.95	0.22	0.926
Feb 25, 2011	10:00	98	34	1.08	0.12	0.887
	14:00	75	25	1.12	0.11	0.902

Increasing AAOD was found to decrease DoLP (N=33, Adjusted R^2=0.31, P<0.001). However, predicting DoLP based on AAOD is less reliable than using PM2.5 mass concentration. In fact, urban cases with higher scattering efficiency can have lower Single Scattering Albedo (SSA) compared to biomass burning and desert cases with the same Aerosol Optical Depth (AOD) but different refractive index (Dubovik *et al.* 2002). Therefore, while SSA (or AAOD) is a useful parameter, it is not a comprehensive variable for predicting DoLP.

In Seoul, the contributions from secondary inorganic aerosols (SNA), organic matter (OM = organic carbon * 1.4), and elemental carbon (EC) are highest in winter, with SNA (especially nitrate) being the dominant component of PM2.5 (Park *et al.* 2018). Ground-based Lidar observations indicated that mineral dust was only a minor source of PM2.5 during our observation period. Using measured mass concentrations of various PM2.5 components (SO_4^{2-}, NO_3^-, Cl^-, Na^+, NH_4^+, K^+, Mg^{2+}, Ca^{2+}, OC, EC, S, K, Ca, Ti, V, Cr, Mn, Fe, Ni, Cu, Zn, As, Se, Br and Pb), Lasso regression models were constructed to select the best model for predicting celestial DoLP. It should be noted that due to missing values, only 27 cases were included in the model. The selected best model includes NO_3^-, Cl^-, EC, and OC as predictors.

Additionally, when building a regression model to predict DoLP using mass concentrations of SNA, OM, and BC, high multicollinearity was observed between OM and EC (VIF>10). Therefore, the relative contribution of increased mass concentrations of $NO_3^{-,}$ Cl-, and EC to DoLP was analyzed using a GLM with a Gamma distribution and log link function. The model including EC showed a better AIC value than the model including OM. Due to the skewness of data at low PM2.5 concentrations, the GLM model was chosen. The results indicated that, in our observations, NO_3^- alone can predict DoLP (Table 8). Figure 11 illustrates the decrease in DoLP as a function of increasing NO_3^-. Furthermore, the results showed that a unit increase in EC could lead to a greater decrease in the mean DoLP value compared to SNA. This suggests that when the proportion of EC is higher than that of SNA in the total PM2.5, the DoLP can be significantly reduced. Although uncertainties exist, these findings represent the best estimate obtained in our study.

Table 8. Relative contribution of increase in mass concentrations of NO_3^-, Cl^- and OC analyzed by GLM (Maximum DoLP = NO_3^- + Cl^- + EC , family = Gamma (link = log).

	Estimate	Std. Error	t-value	*p* value
(Intercept)	4.00	0.036	111.518	
NO_3^-	-0.008	0.004	-2.026	**<0.1**
Cl^-	-0.095	0.090	-1.053	0.301
OC	-0.016	0.014	-1.123	0.271

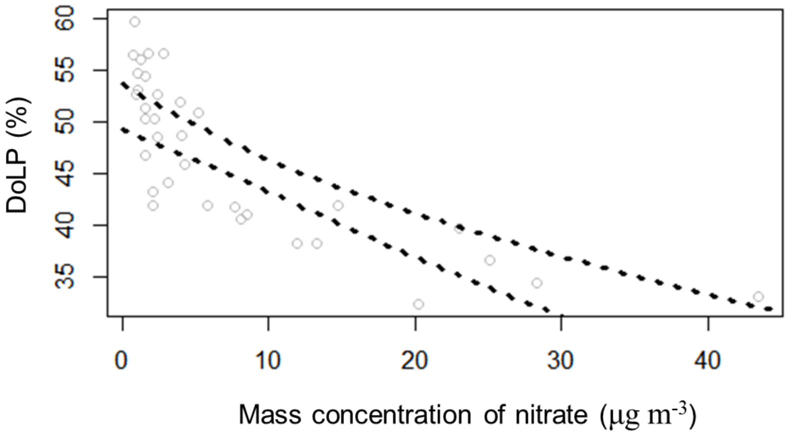

Figure 11. Estimated effect of nitrate alone mass concentration (μg m^{-3}) on the DoLP.

The proportion of absorbing aerosols, specifically EC, in the total PM2.5 is lower during winter in Seoul compared to scattering aerosols (Kim *et al.* 2018). In our analysis, the mass concentration of EC accounted for approximately 1.2-13% of the total PM2.5. The annual average value of EC in East Asian countries generally does not exceed 10%, while it can exceed 20% in African countries and Indian regions (Cheng *et al.* 2016; Snider *et al.* 2016). Therefore, the PM2.5 mass concentration-DoLP model in this study is particularly applicable to cases, especially in urban areas, where SNA dominate PM2.5. Since no Asian dust event occurred during our ground observation period, any effect of mineral dust was not analyzed. However, on January 8, 2023, it was possible to conduct an additional DoLP observation when dust particles were the dominant component of PM2.5 (as determined by ground-based Lidar observation). The PM2.5 mass concentration was 56 $\mu g\ m^{-3}$, and the observed DoLP was 36.9%. According to our model, the predicted range of DoLP was 38.5-42.2%. The observed DoLP was slightly lower than the predicted DoLP. Considering that the DoLP in Beijing was close to zero when the city was covered by a dust storm (AOD_{440}=2.7, PM2.5 mass concentration=193 $\mu g\ m^{-3}$), the impact of dust particles should be at least comparable to that of SNA and Elemental Carbon (EC). Additionally, a previous study demonstrated that, under the same AOD_{450} the DoLP in a desert area is estimated to be lower than that in an urban area (Kreuter *et al.* 2010). Thus, the PM2.5-DoLP model in this study gives rather higher estimates.

3.3 Potential impact of future air quality change on the visual navigation of honey bee

3.3.1 Global changes in the spatial extent of risk hotspots and the frequency of limited-visibility days

Annual total changes in spatial extent of risk hotspots and frequency of limited-visibility days (LVD) per hotspot in 2050 relative to 2010 are different by region and country (see Appendix 1 for classification of region and country). In 2010, the risk hotspots identified by the LB and UB estimations were predominantly captured in Sub-Saharan Africa (Figure 12a, b, respectively). This region already experienced high PM2.5 mass concentration and had many risk hotspots in 2010; therefore, the high PM2.5 is expected to persist in 2050 (Table 9), with no remarkable increase in the frequency of LVD. PM2.5 is expected to increase significantly by 2050 in India and China (Figure 12c, d), two countries contributing over 40% to the total spatial increase in hotspots with increased LVD frequency in 2050, compared to that in 2010 (Figure 12e, f and Tables 10, 11). Over northern India, the frequency of LVD for honey bees is expected to increase by at least 100 days, as per the LB estimation. Further, some parts of the northeastern regions of China will experience an increase of more than 20 days in the frequency of LVD. Although the predicted increase in the LVD frequency is less pronounced in the UB estimation than that in the LB estimation, the LVD frequency in most of northern India is estimated to increase by more than 20 days (up to 103 days, Table 13). Between 2010 and 2050, the frequency of LVD in the Sub-Saharan region is predicted to be generally less than 10 days (Figure 12c, d); however, some countries, such as Chad, Niger, and Algeria, present the most challenging environments for honey bees where they can be perturbed during flight almost year-round as per both estimations. In addition, both estimations captured the largest increase in the maximum number of LVD to occur in Bangladesh and Egypt following India (Tables 12, 13).

Almost every hotspot captured in 2010 is estimated to either maintain the status quo or experience an increase in the number of LVD by at least one day in 2050 (Figure 12e, f). In contrast, very few hotspots will experience a decrease in the number of LVD. Based on the LB estimation for 2050, the frequency of LVD will increase by at least one day over a 14.6 M km^2 area that includes newly emerging hotspots. Of note, risk hotspots of 13.4 M km^2 may experience no change in the number of LVD. Further, larger areas are expected to have no change as shown by the UB estimation. However, risk hotspots of 4.4 M km^2 are to experience an increase in the frequency of LVD.

Overall, the LB estimation shows that by 2050, the risk hotspots will be globally distributed over an area of approximately 28 M km^2, which is almost the size of Africa, a 20% increase in the spatial extent of hotspots from that in 2010 will occur (Table 14). The UB estimation shows a more desirable result, where the risk hotspots will be distributed over approximately 10 M km^2, with a 16% spatial increase between 2010 and 2050 (Table 14).

Since seasonality is a crucial factor in the dynamics of plant-pollinator interactions (Rabeling *et al.* 2019; Martins *et al.* 2021), Figure 13a and Figure 13b further demonstrate the seasonal variability of the increases in the LVD frequency evaluated by the LB and UB estimations, respectively. Here, regions where risk hotspots are dominant, namely Africa, the Eastern Mediterranean, South-Eastern Asia, and Western Pacific, were the focus. At the global scale, the greatest spatial expansion accompanied by increase in the frequency of LVD is expected to occur in December-January-February (DJF), followed by March-April-May

(MAM), September-October-November (SON), and June-July-August (JJA) as per the LB estimation, and DJF followed by SON, MAM, and JJA as per the UB estimation (Table 15). The spatial extent of risk hotspots in 2050 is expected to be the greatest in DJF, followed by SON, MAM, and JJA in both estimations. It is noteworthy that while much smaller number of the risk hotspots are captured in JJA compared to the other seasons, honey bees in E. Mediterranean countries are still likely to experience limited visibility for more than 10 days on average during this season. The likely range of LVD frequencies for each season in 2050 (within the 95% lower and upper CIs of the PM2.5 thresholds for each LB and UB estimation) and the impacted areas are shown in Figure 14.

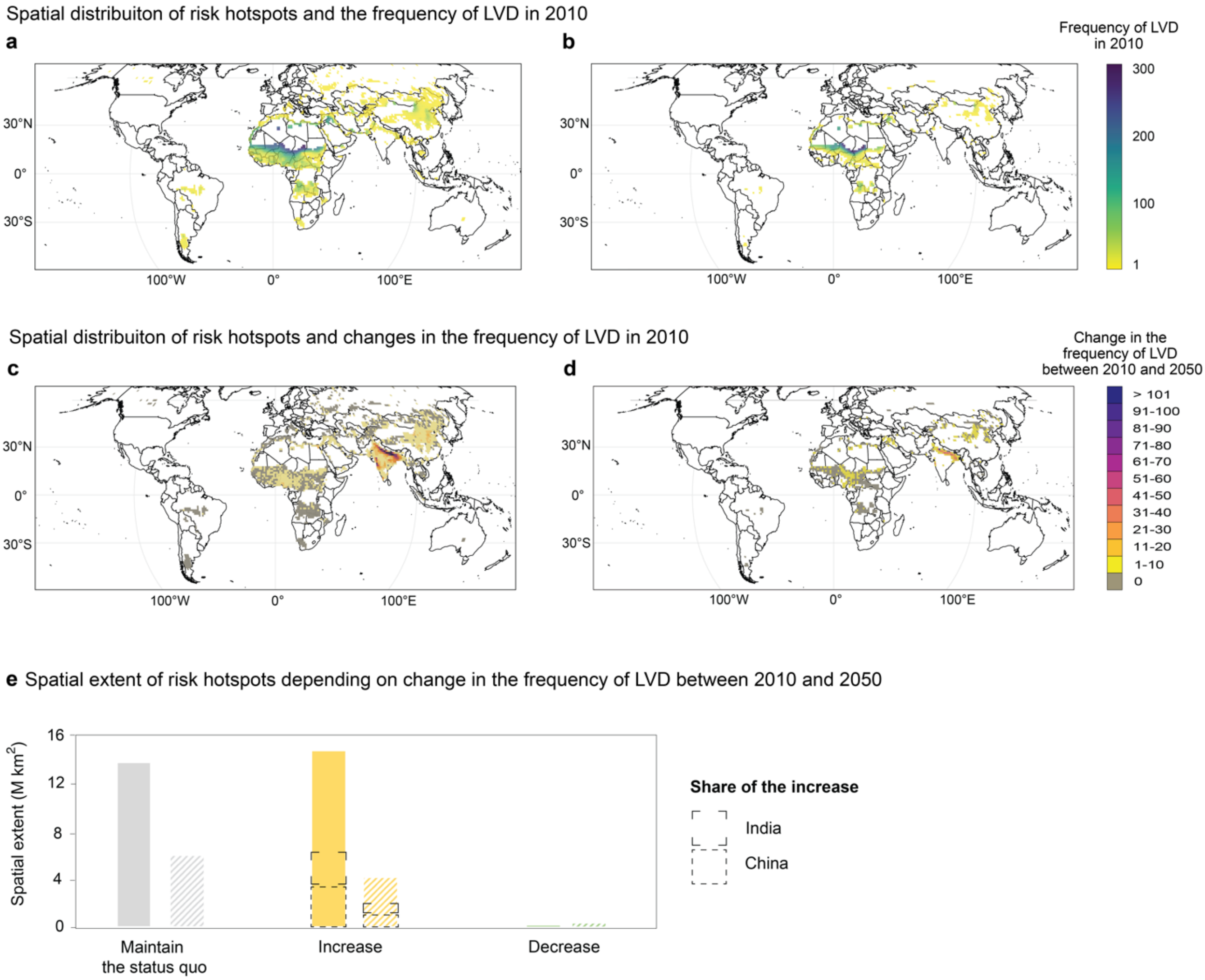

Figure 12. Global distribution of risk hotspots and annual total frequency of LVD as the number of LVD days per risk hotspot in 2010, as evaluated by the LB and UB estimations (a and b). Changes in the annual total frequency of LVD in 2050 compared to that in 2010 (c and d). The estimated spatial extent of risk hotspots where no change (status quo), increase, or decrease in the frequency of LVD is expected in 2050 (e). Bars with solid fill and oblique line fill represent LB and UB estimations, respectively. Note that hotspots where decreases in the frequency of LVD expected (<0 in c and d) are very few so that they are unnoticeable in the maps.

Table 9. Total spatial extent of risk hotspots by country and region projected in the LB and UB estimations in 2050.

Country	Extent (km^2)	
India	2,602,000	745,000
Myanmar	292,000	44,000
Indonesia	140,000	16,000
Bangladesh	129,000	71,000
Thailand	104,000	30,000
Nepal	14,000	-
China	5,206,000	1,985,000
Mongolia	597,000	186,000
Cambodia	152,000	46,000
Vietnam	59,000	15,000
Laos	59,000	15,000
Australia	55,000	-
North Korea	36,000	-
South Korea	13,000	-
Democratic Republic of the Congo	1,037,000	526,000
Sudan	955,000	468,000
Nigeria	891,000	583,000
Mali	783,000	540,000
Chad	700,000	685,000
Angola	673,000	323,000
Central African Republic	635,000	449,000
South Sudan	572,000	217,000
Niger	527,000	527,000
Cameroon	341,000	232,000
Zambia	336,000	61,000
Mauritania	313,000	313,000

Algeria	297,000	106,000
Burkina Faso	259,000	183,000
Ivory Coast	247,000	15,000
Ghana	216,000	77,000
Guinea	215,000	31,000
Senegal	212,000	45,000
South Africa	201,000	-
Mozambique	165,000	30,000
Benin	108,000	15,000
Togo	77,000	15,000
Namibia	69,000	-
Uganda	62,000	-
Sierra Leone	62,000	15,000
Republic of the Congo	47,000	-
United Republic of Tanzania	46,000	-
Somaliland	46,000	-
Ethiopia	31,000	-
Eritrea	30,000	-
Liberia	15,000	-
Guinea Bissau	15,000	-
Malawi	15,000	-
Pakistan	460,000	108,000
Iraq	324,000	221,000
Morocco	312,000	154,000
Iran	270,000	93,000
Afghanistan	242,000	38,000
Libya	228,000	215,000
Saudi Arabia	154,000	27,000
Syria	127,000	76,000
Egypt	121,000	107,000

Yemen	120,000	-
Tunisia	64,000	13,000
United Arab Emirates	43,000	-
Oman	14,000	-
Kuwait	14,000	-
Jordan	13,000	-
Lebanon	13,000	-
Russia	1,828,000	211,000
Kazakhstan	665,000	84,000
Turkmenistan	216,000	36,000
Kyrgyzstan	188,000	93,000
Turkey	159,000	12,000
Italy	141,000	-
Tajikistan	98,000	12,000
Romania	75,000	-
Ukraine	51,000	10,000
Greece	37,000	-
Uzbekistan	35,000	-
Republic of Serbia	34,000	-
Azerbaijan	24,000	-
Hungary	21,000	11,000
Israel	13,000	-
Slovakia	10,000	-
Canada	87,000	-
United States of America	7,000	-
Brazil	690,000	138,000
Argentina	394,000	68,000
Bolivia	75,000	-
Paraguay	29,000	-

Table 10. List of top 10 countries that account for a major part of the global increase in the spatial extent of the hotspots where the number of LVD are projected to increase by at least one day in 2050 relative to 2010 in the LB estimation.

Country	Extent (M km^2)
China	3.8
India	2.6
Nigeria	0.8
Russia	0.5
Sudan	0.5
Pakistan	0.4
Chad	0.4
Mali	0.4
Iraq	0.3
Central African Republic	0.3

Table 11. List of top 10 countries that account for a major part of the global increase in the spatial extent of the hotspots where the number of LVD are projected to increase by at least one day in 2050 relative to 2010 in the UB estimation.

Country	Extent (M km^2)
China	1.1
India	0.7
Nigeria	0.4
Niger	0.3
Chad	0.3
Sudan	0.2
Cameroon	0.2
Iraq	0.2
Libya	0.1
Mali	0.1

Table 12. List of top 30 countries that are to have the greatest peak in changes in the frequency of LVD per risk hotspot projected in the LB estimation. Increase in the number of days relative to 2010 is given. Top three countries with the highest value for each column are in bold.

Country	Max. number of days	(+) Δ from 2010
Chad	**316**	1
Niger	**272**	0
Algeria	**250**	0
Mali	223	2
Sudan	211	4
Nigeria	207	0
Mauritania	185	0
Libya	184	1
Iraq	176	4
India	169	**129**
Cameroon	167	0
Morocco	156	0
Egypt	154	**28**
Burkina Faso	139	1
Saudi Arabia	125	4
Senegal	115	0
Syria	112	9
Iran	110	3
Bangladesh	91	**64**
Pakistan	90	20
Democratic Republic of the Congo	82	0
China	81	4
Mongolia	77	2

Yemen	73	4
Angola	70	0
Guinea	65	1
Turkmenistan	63	2
Ghana	58	0
Central African Republic	57	0
Togo	49	1

Table 13. List of top 30 countries that are to have the greatest peak in changes in the frequency of LVD per risk hotspot projected in the UB estimation. Increase in the number of days relative to 2010 is given. Top three countries with the highest value for each column are in bold.

Country	**Max. number of days**	**(+)** Δ from 2010
Chad	**225**	1
Niger	**214**	0
Nigeria	**152**	1
Mali	117	0
Algeria	115	1
India	106	**103**
Cameroon	89	3
Libya	81	1
Mauritania	65	1
Iraq	61	1
Morocco	57	1
Sudan	53	2
Democratic Republic of the Congo	50	0
China	49	1
Angola	47	0
Egypt	40	**10**
Bangladesh	37	**37**
Mongolia	32	2
Burkina Faso	30	0
Syria	27	3
Ghana	26	0
Saudi Arabia	26	0
Iran	24	0
Senegal	18	0

Central African Republic	13	0
Zambia	13	0
Brazil	10	0
Pakistan	6	2
Tunisia	6	0
Benin	5	0

Table 14. Spatial extent of risk hotspots in 2050 and changes in the extent between 2010 and 2050 globally.

Region	LB estimation		UB estimation	
	Spatial extent of risk hotspots in 2050 (km^2)	Δ between 2010 – 2050 (%)	Spatial extent of risk hotspots in 2050 (km^2)	Δ between 2010 – 2050 (%)
Global	28,095,000	20.0	10,338,000	16.0

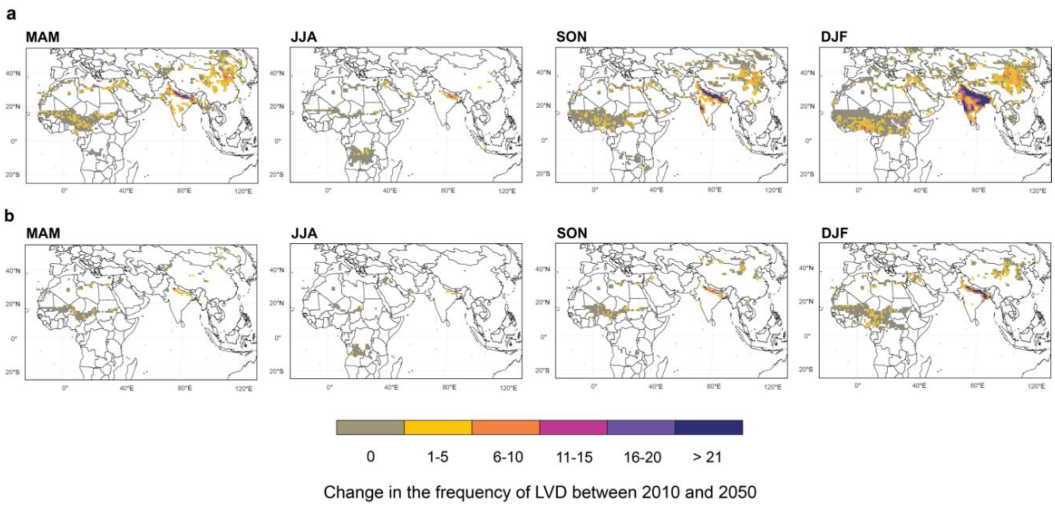

Figure 13. Seasonal variability in the change in frequency of LVD between 2050 and 2010, evaluated by the LB estimation (a) and the UB estimation (b).

Table 15. Seasonal changes in the spatial extent of risk hotspots in 2050 and changes in the spatial extent of risk hotspots of increasing LVD frequency in 2050 relative to 2010 projected in the LB and UB estimations.

Season	**LB projection**		**UB projection**	
	Spatial extent of risk hotspots in 2050 (km^2)	Spatial extent of risk hotspots of increasing frequency of LVD (km^2)	Spatial extent of risk hotspots in 2050 (km^2)	Spatial extent of risk hotspots of increasing frequency of LVD (km^2)
MAM	12,345,000	6,090,000	3,268,000	869,000
JJA	5,719,000	903,000	1,874,000	203,000
SON	13,869,000	5,687,000	4,203,000	1,419,000
DJF	21,257,000	10,330,000	8,525,000	3,114,000

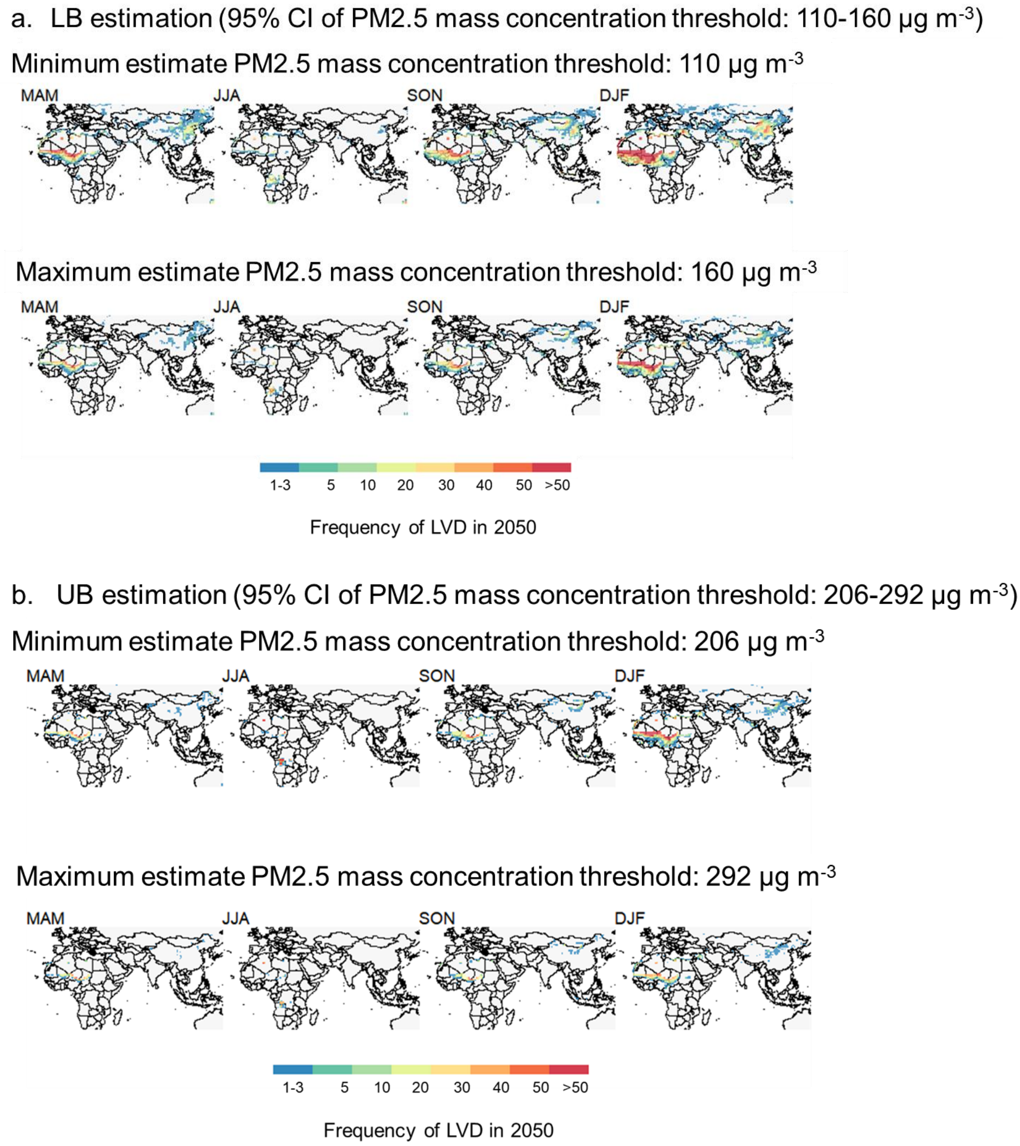

Figure 14. The likely range of LVD frequencies for each season in 2050 based on the obtained 95% CIs of PM2.5 mass concentration thresholds of each LB and UB estimation (in panel a and b, respectively).

3.3.2 Predominant expansion of limited-visibility risk in India and China

India and China are major contributors to the spatial expansion of risk hotspots where honey bees may experience increases in the frequency of LVD (Table 11, 12). In India, the total area of the risk hotspots by the LB estimation is expected to be 2.6 M km^2 in 2050 (Table 9), which is an estimated 5-fold increase from 0.5 M km^2 in 2010 (Figure 15a, compared with Figure 12a). Nearly all risk hotspots of 2010 in India may experience an increase in the number of LVD. The spatial extent of risk hotspots with increased LVD frequency by more than 20 days is greater than that with smaller increments, accounting for approximately 30% of the country's vegetated land surface. Overall, 90% of the vegetated land surface is expected to undergo an increase in the frequency of LVD in the LB estimation. According to the UB estimation, the spatial extent of risk hotspots in 2050 is expected to be 0.7 M km^2 (Table 10) and increases in frequency of LVD will occur in almost every hotspot of 2010.

In China, the total area of risk hotspots is expected to reach 5.2 M km^2 by 2050 (Table 9), which is a 1.13-fold increase relative to the 4.6 M km^2 recorded in 2010 (Figure 15b). Risk hotspots distributed over an area of 3.8 M km^2 (Figure 12a), which accounts for than 80% of the hotspot area compared to that of 2010, will be subjected to an increase in the frequency of LVD. Most risk hotspots that comprise 40% of the total vegetated land surface will be subjected to small increments (1–5 days). Nonetheless, our estimations show that the spatial extent of such risk hotspots (3 M km^2) by size is the greatest among all countries. The UB estimation evaluated that the spatial extent of risk hotspots in 2050 would be 2 M km^2 (Table 10) and increases in the frequency of LVD are expected to occur in 1.1 M km^2 of this area between 2010 and 2050.

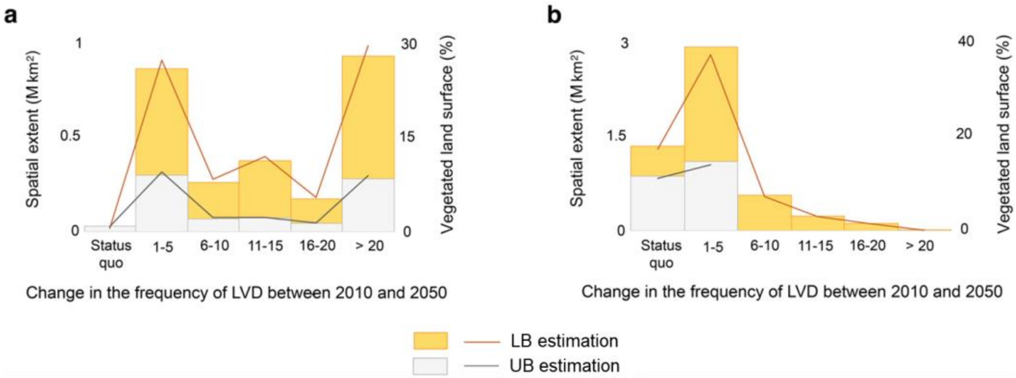

Figure 15. Changes in the spatial extent corresponding to different ranges of increases in the frequency of LVD in 2050 estimated in the LB and UB estimations. a: India, b: China. Bars in the graphs represent spatial extent (primary axis), and solid lines demonstrate the percentage of the spatial extent to the total vegetated land surface of each country (secondary axis).

4. Summary and Discussion

In Chapter 3.1, the results of colony monitoring using RFID clearly demonstrated a strong association between foraging trip duration and PM2.5 mass concentration. This indicates that days with high PM2.5 mass concentrations can significantly impact honey bee foraging performance, regardless of the occurrence of a major dust storm event. High PM2.5 mass concentrations are characteristic of severe urban pollution days.

While the relationship between PM2.5 and DoLP has been discussed in a limited number of studies, the effect of wildfires on DoLP reduction due to multiple scattering of smoke aerosols has been highlighted (Hegedüs *et al.* 2007a; Shaw *et al.* 2014). According to a study by Hegedüs et al. found that during a forest fire outbreak, the average DoLP was lower than 8%, which is below the threshold necessary for bee navigation (Hegedüs *et al.* 2007a).

Although the PM2.5 mass concentration alone has a significant effect on foraging duration, this effect is synergistic with overcast skies. The polarization pattern, measured by the angle of polarization, remains relatively consistent under different cloud conditions (Pomozi *et al.* 2001; Hegedüs *et al.* 2007b). However, the DoLP is reduced under overcast skies, indicating limited usefulness of celestial polarization information for bees. In completely overcast skies with thick clouds, the DoLP can drop to zero (Brines & Gould 1982; Pomozi *et al.* 2001). Therefore, it is logical that the effect of PM2.5 mass concentration synergizes with overcast skies, supporting our findings. This implies that honey bees face greater difficulties in navigation under very cloudy skies when air quality is poor.

Furthermore, the results demonstrate that, contrary to our hypothesis, foraging duration increases in cases dominated by anthropogenic pollutants (smaller DR) rather than dust-dominated cases (larger DR). The DR provides valuable information for characterizing the dominant particle type in the atmosphere in terms of their physical shape (Ge *et al.* 2011; Bi *et al.* 2017). During an Asian dust event, non-spherical particles are predominantly present in the atmosphere, and these irregularly shaped mineral particles exhibit a large DR.

DR and size describe different optical properties of PM, larger particles tend to have a larger DR. Empirical studies conducted in Beijing showed that the average hourly and monthly DR for coarse particles with an optical size (Dp) of 5 μm was higher than that for fine particles with Dp of 1 μm (Tian *et al.* 2018). The DoLP depends greatly on the size of scattering particles (Schechner *et al.* 2003), and larger particles are less effective in terms of depolarization. Light scattering for a given mass concentration of PM increases with decreasing particle size (Hinds 1999). Therefore, our visibility is also influenced by fine mode PM (ranging from 0.1 – 2 μm). The microphysical properties of fine mode particles strongly affect the DoLP of a cloudless sky (Boesche *et al.* 2006). Thus, the effects of DR and PM2.5 mass concentration on foraging duration can counteract each other.

This finding is consistent with a study exploring how different combinations of aerosol mode and AOD influence the DoLP. Over land surfaces with a given AOD, the average DoLP of fine mode particles is lower than that of coarse mode particles characterized as polluted dust (Chen *et al.* 2020). Additionally, in both coarse and fine modes, the DoLP is reduced as AOD increases (Chen *et al.* 2020). Taken together with our results, it is the mass concentration of fine mode particles rather than the dominant morphology that is important in determining the DoLP of the sky. This could explain why foraging duration does not increase with increasing DR in our study. However, when foraging trip duration was regressed on DR only (alongside meteorological variables) in our study, DR did not show any significant effect, while the opposite was true for PM2.5 mass concentration (Table 6). Therefore, the mass concentration of PM2.5 overrides the effect of DR on honey bee foraging performance.

In an experimental study, it was observed that disoriented colonies had significantly longer average foraging durations compared to oriented colonies (I'Anson Price *et al.* 2019). The increased trip duration observed in our study during a heavy air pollution episode can be attributed to the complexity of visual cues, as expected. In an experimental study, it was observed that disoriented colonies had significantly longer average foraging durations compared to oriented colonies (I'Anson Price *et al.* 2019). The increased trip duration observed in our study during a heavy air pollution episode can be attributed to the complexity of visual cues, as expected. Further, although it was unable to quantify this precisely, it is notable that a few observations during DS (degraded air quality conditions) indicated that forager bees either disappeared after attempting outbound trips or did not initiate foraging in the first place.

It is noteworthy that the foraging duration of forager bees did not return to pre-dust storm levels after the dust storm. Despite the average PM2.5 mass concentration during the post-dust storm period (49 μg m^{-3}) being as low as that during the pre-dust storm period (48 μg m^{-3}), the bees still spent 32 minutes more in foraging. This may be attributed to physical damage they incurred and the low quality of food foraged during the dust event. Although variations in the quality or availability of floral resources throughout the study period were not investigated, a causal link between foraging trip duration and resource availability depending on different air quality should be considered in further studies. Foragers frequently encounter airborne PM, which could lead to poor foraging performance due to exposure to toxic chemical elements (Negri *et al.* 2015).

Additionally, newly-stored (1-day-old) fresh pollen is consumed three times more often than older stored (10-day-old) pollen (Carroll *et al.* 2017). This suggests that a state of malnutrition within the colony may persist if low-quality food resources are stored and consumed for several days. These factors contribute to the acute impacts of poor air quality on bee foraging.

In a recent study conducted in India, where many of the world's most polluted cities are located, significant correlations were found between increases in PM10 and physiological changes in Giant Asian honey bees (*Apis dorsata*) (Thimmegowda *et al.* 2020). Giant Asian honey bees from severely polluted areas in Bangalore, India, exhibited significantly lower survival rates. These bees from highly polluted sites also had higher exposure to toxic metals such as lead (Pb). Serious physical damage to wings, antennae, and hindlegs was observed as well. Furthermore, colony-level chronic impacts through gene expression can be predicted. For example, vitellogenin, associated with the survival of worker bees, was found to be depleted in bees sampled from highly polluted sites compared to those from low-polluted sites (Thimmegowda *et al.* 2020). This is significant because reduced fitness of individual foragers and their colonies due to degraded foraging performance can have detrimental impacts on pollination services. In an additional colony monitoring conducted in 2023, a significant positive correlation was found between ambient PM2.5 mass concentration and inside-hive PM2.5 mass concentration (R^2=0.54, P<0.05). Therefore, it cannot be excluded that the physiological effects of particulate matter on the rest of the bees that stayed inside the hive during a severe pollution episode and did not perform foraging trips.

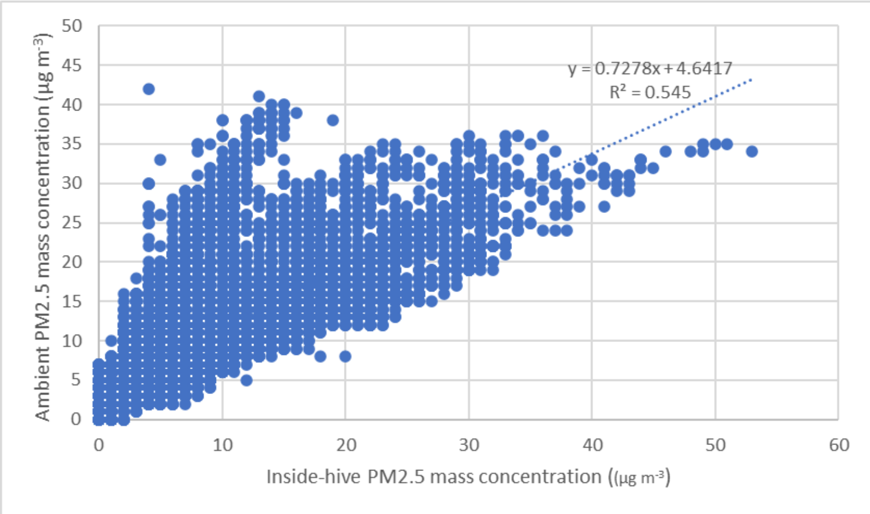

Figure 16. Correlation between ambient PM2.5 mass concentration and inside-hive PM2.5 mass concentration.

The experimental design of this study was constrained due to a severe outbreak of air pollution during the study period. Additionally, it should be noted that our results may not provide a comprehensive analysis of specific air pollutants such as nitrogen dioxide and hydroxyl radicals. For instance, Fuentes *et al*. (2016) examined the impact of air pollutants, including ozone, on floral scents and observed significant degradation of floral volatile compounds even under moderate levels of air pollution. Honey bee foragers experienced delays in locating floral sources even at very low ozone levels (less than 20 parts per billion per volume). However, during episodes of heavy pollution, relatively short durations of sunshine can impede the production of surface ozone by ozone precursors like hydroxyl radicals (Lee *et al.* 2004). Interactions between different types of pollutants can yield diverse effects on honey bee foraging.

In summary, the findings presented in Chapter 3.1 lead us to conclude that the foraging performance of individual honey bees may be hindered by poor air quality. This is the first empirical study to quantitatively assess variations in foraging duration based on air quality while also analyzing the relationship between foraging duration and atmospheric optical properties. Impaired foraging performance can contribute as an additional stressor alongside other factors believed to be the main proximate causes of the global decline in bee populations.

In Chapter 3.2, the aim was to empirically quantify the relationship between atmospheric PM2.5 and the DoLP and utilize this relationship to identify global risk hotspots where honey bees might experience limited visibility during flight. Statistical analyses estimated two threshold levels of PM2.5 mass concentrations: 130 μg m^{-3} (lower bound (LB) estimation) and 240 μg m^{-3} (upper bound (UB) estimation). At these thresholds, the DoLP over the sky starts to decrease below the navigational threshold for honey bees. Although the primary dataset was collected between the December solstice and March equinox, it was assumed that these PM2.5 thresholds represent the higher-end estimates overall. This is because higher relative humidity during other seasons can generally reduce the DoLP to levels lower than those estimated in the model. To supplement the analysis, additional DoLP observations were conducted in November 2022 and collected 16 supplementary data points. Using these additional data, a supplementary PM2.5-DoLP model (N=56) was constructed to compare its explanatory power and confidence interval with the original model presented in the manuscript. It is important to note that the ground observation station was relocated to a site approximately 600 meters away from the original site. Consequently, only the maximum DoLP values were estimated for the additional observations. Therefore, the comparison of explanatory powers between the original and supplementary PM2.5-DoLP models was only conducted for the maximum DoLP. Nevertheless, it was assumed that changes in average DoLPs follow similar patterns to those in the maximum DoLPs, as the distribution of DoLP patterns across the sky is highly uniform. Additionally, in the previous analysis, the average and maximum DoLPs exhibited a strong correlation (r=0.90). The explanatory power of the new PM2.5-DoLP model, incorporating the additional observation data, was slightly lower (adjusted R^2=0.69, P value <0.001) than that of the original model (adjusted R^2=0.71, P value<0.001). This slight difference can be attributed to the relocation of the observation site and the slightly extended seasonal range of observation (compared to the original range from the December solstice to the March equinox). However, Figure 2 illustrates that the CI for the PM2.5 threshold, estimated from the supplementary PM2.5-DoLP model, expanded to 199-291 μg m-3, with the lower bound becoming smaller compared to the CI from the original model (206-292 μg m^{-3}). Furthermore, the best-fit threshold based on the upper bound estimation (using the maximum DoLP) is slightly smaller (235 μg m^{-3}) than the thresholds from the original model (240 μg m^{-3}).

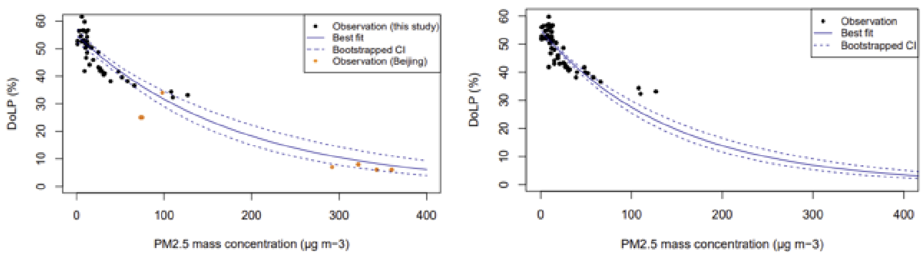

Figure 17. Original PM2.5-DoLP model with data collected in Beijing (left) and supplementary PM2.5-DoLP model incorporating observations in Seoul from 2022 (right).

As demonstrated throughout Chapter 3.3, in an area greater than 10 M km^2 globally, honey bees are expected to experience visual impairment for at least one day in 2050, even under the UB estimation. Countries with stronger regulatory policies on air quality generally have only a few risk hotspots. In contrast, the risk of limited visibility for honey bees is expected to be prevalent in the Sub-Saharan region, India, and China. Furthermore, based on the spatial extent and frequency of limited - visibility days (LVD), the risk is estimated to significantly increase in India and China by 2050. According to our estimations, honey bees in India and China will experience a rapid reduction in clear-sky visibility, impeding their optimal foraging for survival and plant pollination. This situation has serious implications for plant-pollinator interactions in the ecosystem.

Safeguarding the fundamental relationship between plants and pollinators is crucial for agriculture and farming-based livelihoods in various regions (Klein *et al.* 2007; Christmann 2019). Many African and Asian countries are notorious for poor air quality (Akimoto 2003; Baldasano *et al.* 2003). However, their agricultural dependence on bee pollination has been growing over the past few decades (Potts *et al.* 2016; Aizen *et al.* 2019). Among African countries, the socio-economic status of the Sub-Saharan region, especially in areas heavily reliant on pollinator-dependent vegetation production, is significantly threatened (Stein *et al.* 2017; Tibesigwa *et al.* 2019). In Asia, particular attention should be paid to India and China as the potential impacts of worsening air quality on honey bee navigation are expected to be the greatest in these countries by 2050. India is the world's second-largest producer of fruits and vegetables, , with over 70% of the population relying on agriculture as a source of income (Ahmad *et al.* 2011). In some regions, agricultural production dependent on honey bee pollination is active even during the

DJF season, which poses the highest evaluated risk based on our estimations (Bhalchandra *et al.* 2014; Sambasivam *et al.* 2020). China receives the greatest economic benefit from pollination globally, with the northeastern region earning the highest profit (Lautenbach *et al.* 2012). Northeastern China earns the biggest profit (Lautenbach *et al.* 2012). However, this region has been identified as having the maximum number of risk hotspots within the nation in both estimations. Failure to meet the pollination demand for agricultural production in India and China may cause food shortages and global micronutrient deficiency (Ellis *et al.* 2015; Smith *et al.* 2015).

China and India are the two largest recipients of pollination benefits and, coincidentally, the two largest emitters of anthropogenic aerosols (Lu *et al.* 2011; Cheng *et al.* 2016). In recent years, the annual average PM2.5 in many cities in the two countries (e.g., parts of the Indo-Gangetic Plain (van Donkelaar *et al.* 2021), Delhi (Cheng *et al.* 2016), the central Indian region (Massey *et al.* 2009), and the capital city of Hebei Province in China (Brauer *et al.* 2016) have experienced annual average PM2.5 concentrations exceeding the threshold concentrations defined in our analyses.

Note that our estimations are conservative in two ways. First, the measured DoLP values in this study were obtained when secondary inorganic aerosols were dominant, Second, the measured DoLPs represented the maximum DoLPs observed during the day. In the global context, PM2.5 is primarily classified into different components, including SNA (sum of sulfate, nitrate, and ammonium), OM (organic matter), BC (black carbon), dust, and sea salt (Cheng *et al.* 2016). Each type of aerosol has distinct microphysical properties and refractive indices, which influence their extinction efficiency and, consequently, the DoLP (Dubovik *et al.* 2002; Li *et al.* 2022a). The effects of different types of aerosols on PM2.5 during our observations were accounted for in the CIs estimated in our PM2.5 mass concentration-DoLP model. Among the ground-measured metrics, extinction coefficients could serve as the most straightforward variable for predicting the DoLP. However, the statistical relationship between the extinction coefficients and the (maximum) DoLP had a much lower explanatory power (R^2=0.44) compared to the relationship between PM2.5 mass concentrations and the maximum DoLP (R^2=0.72). Notably, when using real measurements of each PM2.5 component during our observations, Lasso regression predicts that a 1 unit increase in OM has a larger effect on the DoLP compared to SNA (see Methods). Given that SNA, especially nitrate, was the dominant component of PM2.5 during the DoLP observation period in our study location (Seoul), the DoLP predicted by PM2.5 mass concentration in other regions, such as the Eastern Mediterranean and India, where the contribution of OM to PM2.5 surpasses that of SNA, may be lower than estimated by the model. In addition, theoretically, the DoLP is maximum when the solar zenith angle (SZA) is 90°, corresponding to sunrise or sunset (Dahlberg *et al.* 2011). As the DoLP exhibits greater sensitivity to smaller SZAs and longer wavelengths (Pust & Shaw 2012; Shaw *et al.* 2014), the DoLP in the blue band (peak sensitivity at 450 nm) was observed during sunrise to enhance accuracy. Although honey bees (*Apis mellifera* in this study) are most sensitive to polarized skylight in the ultraviolet (UV) spectrum (345–360 nm) (Barta & Horváth 2004; Sakura *et al.* 2012; Ogawa *et al.* 2017), there is only a slight qualitative difference between the DoLP values obtained from the blue band and those from the UV band (Pomozi *et al.* 2001; Gassó & Knobelspiesse 2022). In fact, the DoLP in the band can be significantly smaller than that in the blue band, both under clear and polluted sky (Brines & Gould 1982; Coulson 1988; Dahlberg *et al.* 2011; Gassó & Knobelspiesse 2022). It is worth noting that bumblebees (*Bombus hortorum*), another widely distributed bee pollinator, are most sensitive to polarized skylight in the UV and blue (430 nm) spectral regions[88]. Collectively, the expected DoLP based on PM2.5 mass concentrations in different regions and at different times should be lower than that estimates provided by the model in this study.

In conclusion, future air quality deterioration due to rising particulate matter concentrations is primarily influenced by current anthropogenic activities, which have the potential to significantly increase the risk of limited visibility for honey bees and reduce the DoLP across the sky. India and China are the top two countries expected to experience drastic increases in the spatial extent and frequency of LVD. Although this study did not consider the effects of climate change on air quality due to high uncertainty, increasing anthropogenic warming is projected to exacerbate the effect on air quality (Hong *et al.* 2019). For example, increasing extreme fire weather is a widely agreed-upon result of anthropogenic climate change (Touma *et al.* 2021). Any efforts to reduce anthropogenic emissions may potentially be offset by the increased probability of wildfire occurrence, as witnessed in the western United States (McClure & Jaffe 2018). Even with strong mitigation, PM2.5 concentrations in the region are projected to increase. With weak mitigation efforts, PM2.5 mass concentrations in the western US are projected to increase by approximately up to 150 $\mu g\ m^{-3}$ (Xie *et al.* 2022). In addition to fire activity, large-scale circulation changes will alter weather conditions conducive to deadly pollution days (Hong *et al.* 2019). Increases in atmospheric stagnation days accompanied by increasing heat waves and decreasing precipitation in the future are projected to be the main contributors to future PM2.5 increases, even under a medium-low emission scenario (Hong *et al.* 2019). There has been an increasing number of studies discussing the air quality co-benefits of climate change, and vice versa (Nemet *et al*. 2010; West *et al.* 2013; Thompson *et al.* 2014; Vandyck *et al*. 2018; Karlsson *et al*. 2020). Initially, these discussions primarily focused on monetary values related to human health and mitigation implications. However, it is evident that more recent research is now exploring the co-benefits arising from air quality and climate change regulation on the overall welfare of the ecosystem, such as enhancing biodiversity.

Risk hotspots are and will continue to be disproportionately distributed globally. However, the impacts of impaired navigation of honey bees can be transboundary, thereby requiring global cooperation on air quality control. Nonetheless, several precedents have been witnessed with atmospheric PM2.5 reduction, especially under strict regulation, even in the short term, providing an optimistic outlook (Zhang *et al.* 2010; Dhaka *et al.* 2020; Mahato *et al.* 2020; Singh & Chauhan 2020; van Donkelaar *et al.* 2021; Yao *et al.* 2021), providing optimistic outlook. In fact, the implementation of strong clean air actions in China has resulted in recent nationwide improvement in air quality. If this trend continues, the risk of limited visibility in China could be lower than what is presented here (Zhang *et al.* 2019). However, it is important not to underestimate the potential offset of reduction in aerosol precursor emissions by the effects of topography, meteorology, and aerosol interactions, which can lead to increased PM2.5 mass concentrations (Le *et al.* 2020; Li *et al.* 2022c). Unfavorable topography and meteorological conditions often play decisive roles in heavy air pollution throughout China, especially in the Northeast region where many of the estimated limited visibility hotspots are located (Li *et al.* 2022b). Interactions between different airborne pollutants can also promote PM2.5 elevations (Le *et al.* 2020; Li *et al.* 2021). Both aspects were reflected in unexpected increases in PM2.5 mass concentration with substantial reduction in anthropogenic emissions during a preventive lockdown period over China (Le *et al.* 2020). A huge reduction in precursor emissions and the consequential aerosol radiative effect accounted for the enhanced PM2.5 levels by increasing surface ozone. The increase in ozone enhanced atmospheric oxidizing capacity, inducing secondary aerosol formation. In conclusion, the overall dissertation highlight the importance of regulating air quality to safeguard plant-pollinator interactions.

5. Concluding remarks

In this dissertation, compelling evidence was present that that air pollution impairs clear sky visibility for honey bee (*Apis mellifera*), the most versatile pollinator, by reducing the intensity of polarized light. Further, the potential global implications of air quality changes on the visual navigation abilities of honey bees in the year 2050 were identified and estimated. The risk of limited visibility identified here could be an overarching stressor to existing threats to pollinator-plant interactions, such as pesticide use, habitat destruction, parasites, and pathogens that have been widely studied.

Adverse associations between poor air quality, particularly with respect to PM2.5 human health have been extensively investigated in various epidemiological and modeling studies. However, research focusing on the impacts of poor air quality with increasing PM2.5 emission on species other than humans has been limited. In addition, several studies have examined the ecological impacts of changes in radiation levels resulting from atmospheric air pollutants, focusing on plant growth and crop production. However, limited attention has been given to the interactions between light properties and pollutants and their potential effects on plant pollinators. This dissertation provides new insights into the ecological impacts of increasing emission of anthropogenic air pollutants.

References

Ahmad, J., Alam, D., Haseen, M.S. (2011). Impact of climate change on agriculture and food security in India. *International Journal of Agriculture, Environment & Biotechnology*, 4, 129-137.

Aizen, M.A., Aguiar, S., Biesmeijer, J.C., Garibaldi, L.A., Inouye, D.W., Jung, C. et al. (2019). Global agricultural productivity is threatened by increasing pollinator dependence without a parallel increase in crop diversification. *Global Change Biology*, 25, 3516-3527.

Akimoto, H. (2003). Global air quality and pollution. *Science*, 302, 1716-1719.

Allen-Wardell, G., Bernhardt, P., Bitner, R., Burquez, A., Buchmann, S., Cane, J. et al. (1998). The potential consequences of pollinator declines on the conservation of biodiversity and stability of food crop yields. *Conservation Biology*, 8-17.

Alpert, P., Kishcha, P., Kaufman, Y.J. & Schwarzbard, R. (2005). Global dimming or local dimming?: Effect of urbanization on sunlight availability. *Geophysical Research Letters*, 32(17).

Andrews, E., Ogren, J.A., Kinne, S. & Samset, B. (2017). Comparison of AOD, AAOD and column single scattering albedo from AERONET retrievals and in situ profiling measurements. *Atmospheric Chemistry & Physics*, 17, 6041-6072.

Antonelli, A. (2023). Five essentials for area-based biodiversity protection. *Nature Ecology & Evolution*, 7, 630-631.

Arneth, A., Leadley, P., Claudet, J., Coll, M., Rondinini, C., Rounsevell, M.D. et al. (2023). Making protected areas effective for biodiversity, climate and food. *Global Change Biology*, 29, 3883-3894.

Ashman, T.-L. & J. Schoen, D. (1994). How long should flowers live? *Nature*, 371(6500), 788-791.

Baldasano, J.M., Valera, E. & Jiménez, P. (2003). Air quality data from large cities. *Science of The Total Environment*, 307, 141-165.

Barta, A. & Horváth, G. (2004). Why is it advantageous for animals to detect celestial polarization in the ultraviolet? Skylight polarization under clouds and canopies is strongest in the UV. *Journal of Theoretical Biology*, 226, 429-437.

Baveco, J.M., Focks, A., Belgers, D., van der Steen, J.J.M., Boesten, J.J., & Roessink, I. (2016). An energetics-based honeybee nectar-foraging model used to assess the potential for landscape-level pesticide exposure dilution. *PeerJ*, 4, e2293-e2293.

Bhalchandra, W., Baviskar, R., Nikam, T. B. (2014). Diversity of nectariferous and polleniferous bee flora at Anjaneri and Dugarwadi hills of Western Ghats of Nasik district (MS) India. *Journal of Entomology & Zoology Studies*, 2(4), 244-249.

Bi, J., Huang, J., Shi, J., Hu, Z., Zhou, T., Zhang, G. et al. (2017). Measurement of scattering and absorption properties of dust aerosol in a Gobi farmland region of northwestern China–a potential anthropogenic influence. *Atmospheric Chemistry & Physics*, 17, 7775.

Boesche, E., Stammes, P., Ruhtz, T., Preusker, R. & Fischer, J. (2006). Effect of aerosol microphysical properties on polarization of skylight: sensitivity study and measurements. *Applied Optics*, 45, 8790-8805.

Bordier, C., Klein, S., Le Conte, Y., Barron, A.B. & Alaux, C. (2018). Stress decreases pollen foraging performance in honeybees. *Journal of Experimental Biology*, 221, jeb171470.

Brauer, M., Freedman, G., Frostad, J., Van Donkelaar, A., Martin, R.V., Dentener, F. et al. (2016). Ambient air pollution exposure estimation for the global burden of disease 2013. *Environmental Science & Technology,* 50, 79-88.

Breeze, T.D., Gallai, N., Garibaldi, L.A. & Li, X.S. (2016). Economic measures of pollination services: shortcomings and future directions. *Trends in Ecology & Evolution*, 31, 927-939.

Brines, M.L. & Gould, J.L. (1982). Skylight polarization patterns and animal orientation. *Journal of Experimental Biology*, 96, 69-91.

Brown, M.J., Dicks, L.V., Paxton, R.J., Baldock, K.C., Barron, A.B., Chauzat, M.-P. et al. (2016). A horizon scan of future threats and opportunities for pollinators and pollination. *PeerJ*,4, e2249.

Burney, J. & Ramanathan, V. (2014). Recent climate and air pollution impacts on Indian agriculture. *Proceedings of the National Academy of Sciences*, 111, 16319-16324.

Cappa, F., Petrocelli, I., Dani, F.R., Dapporto, L., Giovannini, M., Silva-Castellari, J. et al. (2019). Natural biocide disrupts nestmate recognition in honeybees. *Scientific Reports*, 9, 3171.

Carroll, M.J., Brown, N., Goodall, C., Downs, A.M., Sheenan, T.H. & Anderson, K.E. (2017). Honey bees preferentially consume freshly-stored pollen. *PLOS ONE*, 12, e0175933-e0175933.

Chee, Y.E. (2004). An ecological perspective on the valuation of ecosystem services. *Biological Conservation*, 120, 549-565.

Chen, W., Bai, S., Wang, D., Zhao, H., Sun, H., Yi, L. et al. (2020). Aerosol-induced changes in sky polarization pattern: potential hint on applications in polarimetric remote sensing. *International Journal of Remote Sensing*, 41, 4963-4980.

Cheng, Z., Luo, L., Wang, S., Wang, Y., Sharma, S., Shimadera, H. et al. (2016). Status and characteristics of ambient PM2.5 pollution in global megacities. *Environment International*, 89-90, 212-221.

Chowdhury, S., Dey, S. & Smith, K.R. (2018). Ambient PM2.5 exposure and expected premature mortality to 2100 in India under climate change scenarios. *Nature communications*, 9, 318-318.

Chowdhury, S., Pozzer, A., Haines, A., Klingmüller, K., Münzel, T., Paasonen, P. et al. (2022). Global health burden of ambient PM2.5 and the contribution of anthropogenic black carbon and organic aerosols. *Environment International*, 159, 107020.

Christmann, S. (2019). Do we realize the full impact of pollinator loss on other ecosystem services and the challenges for any restoration in terrestrial areas? *Restoration Ecology*, 27, 720-725.

Christmann, S. & Aw-Hassan, A.A. (2012). Farming with alternative pollinators (FAP)—an overlooked win-win-strategy for climate change adaptation.

Agriculture, Ecosystems & Environment, 161, 161-164.
Cohan, D.S., Xu, J., Greenwald, R., Bergin, M.H. & Chameides, W.L. (2002). Impact of atmospheric aerosol light scattering and absorption on terrestrial net primary productivity. *Global Biogeochemical Cycles*, 16(4), 1090, doi:10.1029/2001GB001441
Colin, T., Meikle, W.G., Wu, X. & Barron, A.B. (2019). Traces of a neonicotinoid induce precocious foraging and reduce foraging performance in honey bees. *Environmental Science & Technology*, 53, 8252-8261.
Comino, E. & Marengo, P. (2010). Root tensile strength of three shrub species: *Rosa canina, Cotoneaster dammeri* and *Juniperus horizontalis*: Soil reinforcement estimation by laboratory tests. *CATENA*, 82, 227-235.
Cornelissen, B., Neumann, P. & Schweiger, O. (2019). Global warming promotes biological invasion of a honey bee pest. *Global Change Biology*, 25(11), 3642-3655.
Coulson, K.L. (1988). *Polarization and Intensity of Light in the Atmosphere*. A Deepak Pub.
Dahlberg, A.R., Pust, N.J. & Shaw, J.A. (2011). Effects of surface reflectance on skylight polarization measurements at the Mauna Loa Observatory. *Optics Express*, 19, 16008-16021.
Daily, G.C. (2000). Management objectives for the protection of ecosystem services. *Environmental Science & Policy*, 3, 333-339.
Danner, N., Molitor, A.M., Schiele, S., Härtel, S. & Steffan-Dewenter, I. (2016). Season and landscape composition affect pollen foraging distances and habitat use of honey bees. *Ecological Applications*, 26, 1920-1929.
Degen, J., Kirbach, A., Reiter, L., Lehmann, K., Norton, P., Storms, M. et al. (2015). Exploratory behaviour of honeybees during orientation flights. *Animal Behaviour,* 102, 45-57.
Devi, A. & Satheesh, S.K. (2022). Global maps of aerosol single scattering albedo using combined CERES-MODIS retrieval. *Atmospheric Chemistry & Physics*, 22, 5365-5376.
Dhaka, S.K., Chetna, Kumar, V., Panwar, V., Dimri, A.P., Singh, N. et al. (2020). PM2.5 diminution and haze events over Delhi during the COVID-19 lockdown period: an interplay between the baseline pollution and meteorology. *Scientific Reports*, 10, 13442.
Di Prisco, G., Cavaliere, V., Annoscia, D., Varricchio, P., Caprio, E., Nazzi, F. et al. (2013). Neonicotinoid clothianidin adversely affects insect immunity and promotes replication of a viral pathogen in honey bees. *Proceedings of the National Academy of Sciences*, 110, 18466-18471.
Dirnböck, T., Kraus, D., Grote, R., Klatt, S., Kobler, J., Schindlbacher, A. et al. (2020). Substantial understory contribution to the C sink of a European temperate mountain forest landscape. *Landscape Ecology*, 35, 483-499.
Dovey, K.M., Kemfort, J.R. & Towne, W.F. (2013). The depth of the honeybee's backup sun-compass systems. *Journal of Experimental Biology*, 216, 2129-2139.
Dubovik, O., Holben, B., Eck, T.F., Smirnov, A., Kaufman, Y.J., King, M.D. et al. (2002). Variability of absorption and optical properties of key aerosol types observed in worldwide locations. *Journal of the Atmospheric Sciences*, 59(3),

590-608.
Ellis, A.M., Myers, S.S. & Ricketts, T.H. (2015). Do Pollinators Contribute to Nutritional Health? *PLOS ONE*, 10, e114805.
Emde, C., Buras, R., Mayer, B. & Blumthaler, M. (2010). The impact of aerosols on polarized sky radiance: model development, validation, and applications. *Atmospheric Chemistry & Physics*, 10, 383-396.
Erler, S., Denner, A., Bobiş, O., Forsgren, E. & Moritz, R.F. (2014). Diversity of honey stores and their impact on pathogenic bacteria of the honeybee, *Apis mellifera*. *Ecology and Evolution*, 4, 3960-3967.
Evangelista, C., Kraft, P., Dacke, M., Labhart, T. & Srinivasan, M.V. (2014). Honeybee navigation: critically examining the role of the polarization compass. *Philosophical Transactions of the Royal Society B: Biological Sciences*, 369(1636), 20130037.
Farber, S.C., Costanza, R. & Wilson, M.A. (2002). Economic and ecological concepts for valuing ecosystem services. *Ecological Economics*, 41, 375-392.
Fisogni, A., Hautekèete, N., Piquot, Y., Brun, M., Vanappelghem, C., Michez, D. et al. (2020). Urbanization drives an early spring for plants but not for pollinators. *Oikos*, 129, 1681-1691.
Ford, B., Val Martin, M., Zelasky, S.E., Fischer, E.V., Anenberg, S.C., Heald, C.L. et al. (2018). Future fire impacts on smoke concentrations, visibility, and health in the contiguous United States. *GeoHealth*, 2(8), 229-247.
Foster, J.J., Sharkey, C.R., Gaworska, A.V.A., Roberts, N.W., Whitney, H.M. & Partridge, J.C. (2014). Bumblebees learn polarization patterns. *Current Biology*, 24(12), 1415-1420.
Foster, J.J., Temple, S.E., How, M.J., Daly, I.M., Sharkey, C.R., Wilby, D. et al. (2018). Polarisation vision: overcoming challenges of working with a property of light we barely see. *The Science of Nature*, 105, 1-26.
Fürst, M., McMahon, D.P., Osborne, J., Paxton, R. & Brown, M.J. (2014). Disease associations between honeybees and bumblebees as a threat to wild pollinators. *Nature*, 506, 364-366.
Fuentes, J.D., Chamecki, M., Roulston, T.a., Chen, B. & Pratt, K.R. (2016). Air pollutants degrade floral scents and increase insect foraging times. *Atmospheric Environment*, 141, 361-374.
Gassó, S. & Knobelspiesse, K.D. (2022). Circular polarization in atmospheric aerosols. *Atmospheric Chemistry & Physics*, 22, 13581-13605.
Ge, J., Su, J., Fu, Q., Ackerman, T. & Huang, J. (2011). Dust aerosol forward scattering effects on ground-based aerosol optical depth retrievals. *Journal of Quantitative Spectroscopy & Radiative Transfer*, 112, 310-319.
Gels, J.A., Held, D.W. & Potter, D.A. (2002). Hazards of insecticides to the bumble bees *Bombus impatiens* (Hymenoptera: Apidae) foraging on flowering white clover in turf. *Journal of Economic Entomology*, 95, 722-728.
Gilliam, F.S. (2007). The ecological significance of the herbaceous layer in temperate forest ecosystems. *Bioscience*, 57, 845-858.
Girling, R.D., Lusebrink, I., Farthing, E., Newman, T.A. & Poppy, G.M. (2013). Diesel exhaust rapidly degrades floral odours used by honeybees. *Scientific Reports*, 3, 2779.

Gisder, S., Hedtke, K., Möckel, N., Frielitz, M.C., Linde, A. & Genersch, E. (2010). Five-year cohort study of Nosema spp. in Germany: does climate shape virulence and assertiveness of *Nosema ceranae*? *Applied & Environmental Microbiology*, 76, 3032-3038.

Goulson, D. & Nicholls, E. (2022). Anthropogenic influences on bee foraging. *Science*, 375, 970-972.

Goulson, D., Nicholls, E., Botías, C. & Rotheray, E.L. (2015). Bee declines driven by combined stress from parasites, pesticides, and lack of flowers. *Science*, 347, 1255957.

Hadley, A. S., & Betts, M. G. (2012). The effects of landscape fragmentation on pollination dynamics: absence of evidence not evidence of absence. *Biological Reviews*, 87(3), 526-544.

Hanley, N., Breeze, T.D., Ellis, C. & Goulson, D. (2015). Measuring the economic value of pollination services: Principles, evidence and knowledge gaps. *Ecosystem Services*, 14, 124-132.

Hegedüs, R., Åkesson, S. & Horváth, G. (2007a). Anomalous celestial polarization caused by forest fire smoke: why do some insects become visually disoriented under smoky skies? *Applied Optics*, 46, 2717-2726.

Hegedüs, R., Åkesson, S. & Horváth, G. (2007b). Polarization patterns of thick clouds: overcast skies have distribution of the angle of polarization similar to that of clear skies. *JOSA A*, 24, 2347-2356.

Hegedüs, R., Barta, A., Bernáth, B., Meyer-Rochow, V.B. & Horváth, G. (2007c). Imaging polarimetry of forest canopies: how the azimuth direction of the sun, occluded by vegetation, can be assessed from the polarization pattern of the sunlit foliage. *Applied Optics*, 46, 6019-6032.

Heinrich, B. (1975). Energetics of pollination. *Annual Review of Ecology and Systematics*, 6, 139-170.

Hemberger, J. & Gratton, C. (2018). Floral resource pulse decreases bumble bee foraging trip duration in central Wisconsin agroecosystem. *Ecological Entomology*, 43, 447-457.

Henry, M., Beguin, M., Requier, F., Rollin, O., Odoux, J.-F., Aupinel, P. et al. (2012). A common pesticide decreases foraging success and survival in honey bees. *Science,* 336, 348-350.

Henze, M.J. & Labhart, T. (2007). Haze, clouds and limited sky visibility: polarotactic orientation of crickets under difficult stimulus conditions. *Journal of Experimental Biology*, 210, 3266-3276.

Higginson, A.D., Barnard, C.J., Tofilski, A., Medina, L., Ratnieks, F. (2011). Experimental wing damage affects foraging effort and foraging distance in honeybees *Apis mellifera*. *Psyche: A Journal of Entomology*, 2011, 32.

Hinds, W.C. (1999). Aerosol Technology: Properties, Behavior, and Measurement of Airborne Particles. Second edn. A Wiley-Interscience publication, USA.

Hong, C., Zhang, Q., Zhang, Y., Davis, S.J., Tong, D., Zheng, Y. et al. (2019). Impacts of climate change on future air quality and human health in China. *Proceedings of the National Academy of Sciences*, 116(35), 17193-17200. .

I'Anson Price, R., Dulex, N., Vial, N., Vincent, C. & Grüter, C. (2019). Honeybees forage more successfully without the "dance language" in challenging environments. *Science Advances*, 5, eaat0450.

Imbach, P., Fung, E., Hannah, L., Navarro-Racines, C.E., Roubik, D.W., Ricketts, T.H. et al. (2017). Coupling of pollination services and coffee suitability under climate change. *Proceedings of the National Academy of Sciences*, 114, 10438-10442.

Jin, N., Klein, S., Leimig, F., Bischoff, G. & Menzel, R. (2015). The neonicotinoid clothianidin interferes with navigation of the solitary bee *Osmia cornuta* in a laboratory test. *Journal of Experimental Biology*, 218, 2821-2825.

Johnson, B.R. (2002). Reallocation of labor in honeybee colonies during heat stress: the relative roles of task switching and the activation of reserve labor. *Behavioral Ecology & Sociobiology*, 51, 188-196.

Kacelnik, A., Houston, A.I., Schmid-Hempel, P. (1986). Central-place foraging in honey bees: the effect of travel time and nectar flow on crop filling. *Behavioral Ecology & Sociobiology*, 19, 19-24.

Karlsson, M., Alfredsson, E., & Westling, N. (2020). Climate policy co-benefits: a review. *Climate Policy*, 20(3), 292-316.

Kelber, A. & Somanathan, H. (2019). Spatial vision and visually guided behavior in Apidae. *Insects*, 10, 418.

Kennedy, C.M., Lonsdorf, E., Neel, M.C., Williams, N.M., Ricketts, T.H., Winfree, R. et al. (2013). A global quantitative synthesis of local and landscape effects on wild bee pollinators in agroecosystems. *Ecology Letters*, 16, 584-599.

Khalifa, S.A., Elshafiey, E.H., Shetaia, A.A., El-Wahed, A.A., Algethami, A.F., Musharraf, S.G. et al. (2021). Overview of bee pollination and its economic value for crop production. *Insects*, 12.

Kim, D., Oren, R. & Qian, S.S. (2016). Response to CO_2 enrichment of understory vegetation in the shade of forests. *Global Change Biology*, 22, 944-956.

Kim, H., Zhang, Q. & Heo, J. (2018). Influence of intense secondary aerosol formation and long-range transport on aerosol chemistry and properties in the Seoul Metropolitan Area during spring time: results from KORUS-AQ. *Atmospheric Chemistry & Physics*, 18, 7149-7168.

Kim, S.-W., Yoon, S.-C., Kim, J., Kang, J.-Y. & Sugimoto, N. (2010). Asian dust event observed in Seoul, Korea, during 29–31 May 2008: Analysis of transport and vertical distribution of dust particles from lidar and surface measurements. *Science of The Total Environment*, 408, 1707-1718.

Klein, A.-M., Vaissiere, B.E., Cane, J.H., Steffan-Dewenter, I., Cunningham, S.A., Kremen, C. et al. (2007). Importance of pollinators in changing landscapes for world crops. *Proceedings of the Royal Society of London B: Biological Sciences*, 274, 303-313.

Klein, S., Cabirol, A., Devaud, J.-M., Barron, A.B. & Lihoreau, M. (2017). Why bees are so vulnerable to environmental stressors. *Trends in Ecology & Evolution*, 32, 268-278.

Knight, T., Ashman, T.L., Bennett, J., Burns, J., Passonneau, S. & Steets, J. (2018). Reflections on, and visions for, the changing field of pollination ecology. *Ecology Letters*, 21, 1282-1295.

Koch, H., Brown, M.J.F. & Stevenson, P.C. (2017). The role of disease in bee foraging ecology. *Current Opinion in Insect Science*, 21, 60-67.

Kozlov, M.V. (2022). Population dynamics of herbivorous insects in polluted landscapes. *Current Opinion in Insect Sciences*, 54, 100987.

Kraft, P., Evangelista, C., Dacke, M., Labhart, T. & Srinivasan, M.V. (2011). Honeybee navigation: following routes using polarized-light cues. *Philosophical Transactions of the Royal Society of London B: Biological Sciences*, 366, 703-708.

Kreuter, A., Emde, C. & Blumthaler, M. (2010). Measuring the influence of aerosols and albedo on sky polarization. *Atmospheric Research*, 98, 363-367.

Kreuter, A., Zangerl, M., Schwarzmann, M. & Blumthaler, M. (2009). All-sky imaging: a simple, versatile system for atmospheric research. *Applied Optics*, 48, 1091-1097.

Kumar, R., Barth, M.C., Pfister, G.G., Delle Monache, L., Lamarque, J.F., Archer-Nicholls, S. et al. (2018). How Will Air Quality Change in South Asia by 2050? *Journal of Geophysical Research: Atmospheres*, 123(3), 1840-1864.

La Sorte, F.A., Aronson, M.F., Lepczyk, C.A., Horton, K (2022). Assessing the combined threats of artificial light at night and air pollution for the world's nocturnally migrating birds. *Global Ecology and Biogeography,* 31(5), 912-924.

Labhart, T. (1996). How polarization-sensitive interneurones of crickets perform at low degrees of polarization. Journal of experimental biology. *Journal of Experimental Biology,* 199(7), 1467-1475.

Lach, L., Kratz, M. & Baer, B. (2015). Parasitized honey bees are less likely to forage and carry less pollen. *Journal of Invertebrate Pathology,* 130, 64-71.

Latimer, R.N.C. & Martin, R.V. (2019). Interpretation of measured aerosol mass scattering efficiency over North America using a chemical transport model. *Atmospheric Chemistry & Physics*, 19, 2635-2653.

Lautenbach, S., Seppelt, R., Liebscher, J. & Dormann, C.F. (2012). Spatial and Temporal Trends of Global Pollination Benefit. *PLOS ONE*, 7, e35954.

Le, T., Wang, Y., Liu, L., Yang, J., Yung, Y.L., Li, G. et al. (2020). Unexpected air pollution with marked emission reductions during the COVID-19 outbreak in China. *Science*, 369, 702-706.

Lee, B.-K., Jun, N.-Y. & Lee, H.K.J.A.E. (2004). Comparison of particulate matter characteristics before, during, and after Asian dust events in Incheon and Ulsan, Korea. *Atmospheric Environment*, 38, 1535-1545.

Lee, H.-J., Jo, H.-Y., Kim, S.-W., Park, M.-S. & Kim, C.-H. (2019). Impacts of atmospheric vertical structures on transboundary aerosol transport from China to South Korea. *Scientific Reports*, 9, 1-9.

Lelieveld, J., Barlas, C., Giannadaki, D., Pozzer, A.J.A.C. & Physics (2013). Model calculated global, regional and megacity premature mortality due to air pollution. *Atmospheric Chemistry & Physics*, 13, 7023-7037.

Lelieveld, J., Evans, J.S., Fnais, M., Giannadaki, D. & Pozzer, A. (2015). The contribution of outdoor air pollution sources to premature mortality on a global scale. *Nature*, 525, 367-371.

Li, J., Carlson, B.E., Yung, Y.L., Lv, D., Hansen, J., Penner, J.E. et al. (2022a). Scattering and absorbing aerosols in the climate system. *Nature Reviews*

Earth & Environment, 3, 363-379.

Li, J., Hao, X., Liao, H., Wang, Y., Cai, W., Li, K. et al. (2022b). Winter particulate pollution severity in North China driven by atmospheric teleconnections. *Nature Geoscience*, 15, 349-355.

Li, K., Jacob, D.J., Liao, H., Qiu, Y., Shen, L., Zhai, S. et al. (2021). Ozone pollution in the North China Plain spreading into the late-winter haze season. *Proceedings of the National Academy of Sciences*, 118, e2015797118.

Li, X., Bei, N., Wu, J., Liu, S., Wang, Q., Tian, J. et al. (2022c). The heavy particulate matter pollution during the COVID-19 lockdown period in the Guanzhong Basin, China. *Journal of Geophysical Research: Atmosphere*, 127, e2021JD036191.

Liang, Y., Rudik, I., Zou, E.Y., Johnston, A., Rodewald, A.D. & Kling, C.L. (2020). Conservation cobenefits from air pollution regulation: Evidence from birds. 117, 30900-30906.

Liu, M., Bi, J. & Ma, Z. (2017). Visibility-based PM2.5 concentrations in China: 1957–1964 and 1973–2014. *Environmental Science & Technology*, 51, 13161-13169.

Liu, Y., Wooster, M.J., Grosvenor, M.J., Lim, K.S. & Francis, R.A. (2021). Strong impacts of smoke polluted air demonstrated on the flight behaviour of the painted lady butterfly (*Vanessa cardui* L.). *Ecological Entomology*, 46, 195-208.

Lu, Z., Zhang, Q. & Streets, D.G. (2011). Sulfur dioxide and primary carbonaceous aerosol emissions in China and India, 1996–2010. *Atmospheric Chemistry & Physics*, 11, 9839-9864.

Luan, T., Guo, X., Guo, L. & Zhang, T. (2017). Quantifying the relationship among PM2.5 concentration, visibility and planetary boundary layer height for long-lasting haze and fog-haze mixed events in Beijing city. *Atmospheric Chemistry & Physics*, 1-39.

Lundin, O., Rundlöf, M., Smith, H.G., Fries, I. & Bommarco, R. (2015). Neonicotinoid insecticides and their impacts on bees: a systematic review of research approaches and identification of knowledge gaps. *PLOS ONE*, 10, e0136928.

Mahato, S., Pal, S. & Ghosh, K.G. (2020). Effect of lockdown amid COVID-19 pandemic on air quality of the megacity Delhi, India. *Science of The Total Environment*, 730, 139086.

Mahowald, N. (2011). Aerosol indirect effect on biogeochemical cycles and climate. *Science*, 334, 794-796.

Martin, M.V., Heald, C., Lamarque, J., Tilmes, S., Emmons, L., Schichtel, B.A. et al. (2014). How emissions, climate, and land use change will impact mid-century air quality over the United States: a focus on effects at National Parks. *Atmospheric Chemistry & Physics*, 15(5), 2805-2823.

Martins, A.E., Camargo, M.G.G. & Morellato, L.P.C. (2021). Flowering phenology and the influence of seasonality in flower conspicuousness for bees. *Frontiers in Plant Science*, 11 594538.

Massey, D., Masih, J., Kulshrestha, A., Habil, M., Taneja, A. (2009). Indoor/outdoor relationship of fine particles less than 2.5 μm (PM2. 5) in residential homes locations in central Indian region. *Building & Environment*,

44, 2037-2045.
McClure, C.D. & Jaffe, D.A. (2018). US particulate matter air quality improves except in wildfire-prone areas. *Proceedings of the National Academy of Sciences*, 115(31), 7901-7906.
Miao, Y., Li, J., Miao, S., Che, H., Wang, Y., Zhang, X. et al. (2019). Interaction Between Planetary Boundary Layer and PM2.5 Pollution in Megacities in China: a Review. *Current Pollution Reports*, 5, 261-271.
Mitchell, E.A.D., Mulhauser, B., Mulot, M., Mutabazi, A., Glauser, G. & Aebi, A. (2017). A worldwide survey of neonicotinoids in honey. *Science*, 358(6359), 109-111.
Mok, J., Krotkov, N.A., Torres, O., Jethva, H., Li, Z., Kim, J. et al. (2018). Comparisons of spectral aerosol single scattering albedo in Seoul, South Korea. *Atmospheric Measurement Techniques*, 11, 2295-2311.
Mwebaze, P., Marris, G.C., Brown, M., MacLeod, A., Jones, G. & Budge, G.E. (2018). Measuring public perception and preferences for ecosystem services: A case study of bee pollination in the UK. *Land Use Policy*, 71, 355-362.
Nabhan, G.P. & Buchmann, S.L. (1997). Services provided by pollinators. *Nature's Services: societal dependence on natural ecosystems*. Island press.
Naimi, B. & Araújo, M.B. (2016). sdm: a reproducible and extensible R platform for species distribution modelling. *Ecography*, 39, 368-375.
Negri, I., Mavris, C., Di Prisco, G., Caprio, E. & Pellecchia, M. (2015). Honey Bees (*Apis mellifera*, L.) as Active Samplers of Airborne Particulate Matter. *PLOS ONE*, 10, e0132491.
Nemet, G. F., Holloway, T., & Meier, P. (2010). Implications of incorporating air-quality co-benefits into climate change policymaking. *Environmental Research Letters*, 5(1), 014007.
Nguyen, G.T.H., Shimadera, H., Uranishi, K., Matsuo, T. & Kondo, A. (2019). Numerical assessment of PM2.5 and O_3 air quality in Continental Southeast Asia: Impacts of potential future climate change. *Atmospheric Environment*, 215, 116901.
Ogawa, Y., Ribi, W., Zeil, J. & Hemmi, J.M. (2017). Regional differences in the preferred e-vector orientation of honeybee ocellar photoreceptors. *Journal of Experimental Biology*, 220(9), 1701-1708.
Okubo, S., Yoshiyama, M., Nikkeshi, A., Morimoto, N. & Kimura, K. (2020). Effect of cold narcosis on foraging behavior of European honey bees (*Apis mellifera ligustica*) tracked using a radio-frequency identification (RFID) system. *Journal of Apicultural Research*, 59(5), 1027-1032.
Ollerton, J., Winfree, R. & Tarrant, S. (2011). How many flowering plants are pollinated by animals? *Oikos*, 120, 321-326.
Otto, C.R.V., Zheng, H., Gallant, A.L., Iovanna, R., Carlson, B.L., Smart, M.D. et al. (2018). Past role and future outlook of the Conservation Reserve Program for supporting honey bees in the Great Plains. *Proceedings of the National Academy of Sciences*, 115, 7629-7634.
Pan, X., Uno, I., Wang, Z., Nishizawa, T., Sugimoto, N., Yamamoto, S. et al. (2017). Real-time observational evidence of changing Asian dust morphology with the mixing of heavy anthropogenic pollution. *Scientific Reports*, 7.

Park, S.-M., Song, I.-H., Park, J.S., Oh, J., Moon, K.J., Shin, H.J. et al. (2018). Variation of PM2.5 Chemical Compositions and their Contributions to Light Extinction in Seoul. *Aerosol and Air Quality Research*, 18, 2220-2229.
Perry, C.J., Søvik, E., Myerscough, M.R. & Barron, A.B. (2015). Rapid behavioral maturation accelerates failure of stressed honey bee colonies. *Proceedings of the National Academy of Sciences*, 112, 3427-3432.
Phillips, B.B., Bullock, J.M., Gaston, K.J., Hudson-Edwards, K.A., Bamford, M., Cruse, D. et al. (2021). Impacts of multiple pollutants on pollinator activity in road verges. *Journal of Applied Ecology*, 58, 1017-1029.
Pokhrel, R.P., Wagner, N.L., Langridge, J.M., Lack, D.A., Jayarathne, T., Stone, E.A. et al. (2016). Parameterization of single-scattering albedo (SSA) and absorption Ångström exponent (AAE) with EC / OC for aerosol emissions from biomass burning. Atmospheric Chemistry & Physics, 16, 9549-9561.
Pomozi, I., Horváth, G. & Wehner, R. (2001). How the clear-sky angle of polarization pattern continues underneath clouds: full-sky measurements and implications for animal orientation. *Journal of Experimental Biology*, 204, 2933-2942.
Potts, S.G., Biesmeijer, J.C., Kremen, C., Neumann, P., Schweiger, O. & Kunin, W.E. (2010). Global pollinator declines: trends, impacts and drivers. *Trends in Ecology & Evolution*, 25, 345-353.
Potts, S.G., Imperatriz-Fonseca, V., Ngo, H.T., Aizen, M.A., Biesmeijer, J.C., Breeze, T.D. et al. (2016). Safeguarding pollinators and their values to human well-being. *Nature*, 540, 220-229.
Powney, G.D., Carvell, C., Edwards, M., Morris, R.K.A., Roy, H.E., Woodcock, B.A. et al. (2019). Widespread losses of pollinating insects in Britain. *Nature Communications*, 10, 1018.
Pozzer, A., Meij, A.d., Pringle, K., Tost, H., Doering, U., Aardenne, J. et al. (2012a). Distributions and regional budgets of aerosols and their precursors simulated with the EMAC chemistry-climate model. *Atmospheric Chemistry & Physics*, 12, 961-987.
Pozzer, A., Zimmermann, P., Doering, U., Van Aardenne, J., Tost, H., Dentener, F. et al. (2012b). Effects of business-as-usual anthropogenic emissions on air quality. *Atmospheric Chemistry & Physics*, 12, 6915-6937.
Proctor, E., Nol, E., Burke, D. & Crins, W.J. (2012). Responses of insect pollinators and understory plants to silviculture in northern hardwood forests. *Biodiversity and Conservation*, 21, 1703-1740.
Proctor, J. (2021). Atmospheric opacity has a nonlinear effect on global crop yields. *Nature Food*, 2(3), 166-173.
Pust, N.J. & Shaw, J.A. (2012). Wavelength dependence of the degree of polarization in cloud-free skies: simulations of real environments. *Optics Express*, 20, 15559-15568.
Rabeling, S.C., Lim, J.L., Tidon, R., Neff, J.L., Simpson, B.B. & Pawar, S. (2019). Seasonal variation of a plant-pollinator network in the Brazilian Cerrado: Implications for community structure and robustness. *PLOS ONE*, 14, e0224997.
Rader, R., Reilly, J., Bartomeus, I. & Winfree, R. (2013). Native bees buffer the negative impact of climate warming on honey bee pollination of watermelon

crops. *Global Change Biology*, 19, 3103-3110.
Reitmayer, C.M., Ryalls, J.M.W., Farthing, E., Jackson, C.W., Girling, R.D. & Newman, T.A. (2019). Acute exposure to diesel exhaust induces central nervous system stress and altered learning and memory in honey bees. *Scientific Reports*, 9, 5793.
Ricketts, T.H., Regetz, J., Steffan-Dewenter, I., Cunningham, S.A., Kremen, C., Bogdanski, A. et al. (2008). Landscape effects on crop pollination services: are there general patterns? *Ecology letters*, 11, 499-515.
Roberts, J.M.K., Anderson, D.L. & Durr, P.A. (2017). Absence of deformed wing virus and Varroa destructor in Australia provides unique perspectives on honeybee viral landscapes and colony losses. *Scientific Reports*, 7, 6925.
Rodell, M., Houser, P.R., Jambor, U., Gottschalck, J., Mitchell, K., Meng, C.J. et al. (2004). The Global Land Data Assimilation System. *Bulletin of the American Meteorological Society*, 85, 381-394.
Rossel, S. (1993). Navigation by bees using polarized skylight. *Comparative Biochemistry and Physiology Part A: Physiology*, 104, 695-708.
Rossel, S. & Wehner, R. (1982). The Bee's Map of the e-Vector Pattern in the Sky. *Proceedings of the National Academy of Sciences*, 79(14), 4451-4455.
Rossel, S. & Wehner, R. (1984). How bees analyse the polarization patterns in the sky. *Journal of Comparative Physiology A*, 154, 607-615.
Sakura, M., Okada, R. & Aonuma, H. (2012). Evidence for instantaneous e-vector detection in the honeybee using an associative learning paradigm. *Proceedings of the Royal Society B: Biological Sciences*, 279(1728), 535-542.
Sambasivam, V.P., Thiyagarajan, G., Kabir, G., Ali, S.M., Khan, S.A.R. & Yu, Z. (2020). Selection of Winter Season Crop Pattern for Environmental-Friendly Agricultural Practices in India. *Sustainability*, 12, 4562.
Sanchez-Bayo, F. & Goka, K. (2014). Pesticide residues and bees–a risk assessment. *PLOS ONE*, 9, e94482.
Sanderfoot, O.V. & Holloway, T. (2017). Air pollution impacts on avian species via inhalation exposure and associated outcomes. *Environmental Research Letters*, 12(8), 083002.
Schechner, Y.Y., Narasimhan, S.G. & Nayar, S.K.J.A.o. (2003). Polarization-based vision through haze. *Applied Optics*, 42(3), 511-525.
Schwarz, J.P., Stark, H., Spackman, J.R., Ryerson, T.B., Peischl, J., Swartz, W.H. et al. (2009). Heating rates and surface dimming due to black carbon aerosol absorption associated with a major U.S. city. *Geophysical Research Letters*, 36(15), L15807.
Schwarz, M., Folini, D., Yang, S., Allan, R.P. & Wild, M. (2020). Changes in atmospheric shortwave absorption as important driver of dimming and brightening. *Nature Geoscience*, 13, 110-115.
Shaw, J.A., Pust, N.J. & Forbes, E. (2014). Effects of wildfire smoke on atmospheric polarization. In: *Polarization: Measurement, Analysis, and Remote Sensing XI*. International Society for Optics and Photonics, p. 909907.
Shimizu, A., Nishizawa, T., Jin, Y., Kim, S.-W., Wang, Z., Batdorj, D. et al. (2016). Evolution of a lidar network for tropospheric aerosol detection in

East Asia. *Optical Engineering*, 56, 1-12, 12.
Singh, A., Bloss, W.J., Pope, F.D. (2017). 60 years of UK visibility measurements: impact of meteorology and atmospheric pollutants on visibility. *Atmospheric Chemistry & Physics*, 17(3), 2085-2101.
Singh, R.P. & Chauhan, A. (2020). Impact of lockdown on air quality in India during COVID-19 pandemic. *Air Quality, Atmosphere & Health*, 13, 921-928.
Smith, M.R., Singh, G.M., Mozaffarian, D. & Myers, S.S. (2015). Effects of decreases of animal pollinators on human nutrition and global health: a modelling analysis. *The Lancet*, 386, 1964-1972.
Snider, G., Weagle, C.L., Murdymootoo, K.K., Ring, A., Ritchie, Y., Stone, E. et al. (2016). Variation in global chemical composition of PM2.5: emerging results from SPARTAN. *Atmospheric Chemistry & Physics*, 16, 9629-9653.
Srinivasan, M.V. (2011). Honeybees as a Model for the Study of Visually Guided Flight, Navigation, and Biologically Inspired Robotics. *Physiological Reviews*, 91, 413-460.
Stanley, D.A., Garratt, M.P.D., Wickens, J.B., Wickens, V.J., Potts, S.G. & Raine, N.E. (2015). Neonicotinoid pesticide exposure impairs crop pollination services provided by bumblebees. *Nature*, 528, 548-550.
Steffan-Dewenter, I., Potts, S.G., Packer, L. (2005). Pollinator diversity and crop pollination services are at risk. Trends in Ecology & Evolution, 20(12), 651-652.
Stein, K., Coulibaly, D., Stenchly, K., Goetze, D., Porembski, S., Lindner, A. et al. (2017). Bee pollination increases yield quantity and quality of cash crops in Burkina Faso, West Africa. *Scientific Reports*, 7, 17691.
Stout, J.C., Murphy, J.T. & Kavanagh, S. (2019). Assessing market and non-market values of pollination services in Ireland (Pollival). *Environmental Protection Agency Research Report, Johnstown Castle, Co. Wexford, Ireland https://www. epa. ie/publications/research/biodiversity/Research_Report_291. pdf.*
Streets, D.G., Wu, Y. & Chin, M. (2006). Two-decadal aerosol trends as a likely explanation of the global dimming/brightening transition. *Geophysical Research Letters*, 33.
Søvik, E., Perry, C.J., LaMora, A., Barron, A.B. & Ben-Shahar, Y. (2015). Negative impact of manganese on honeybee foraging. *Biology Letters*, 11(3), 20140989.
Tan, Y.Q., Dion, E. & Monteiro, A. (2018). Haze smoke impacts survival and development of butterflies. *Scientific Reports*, 8, 15667-15667.
Team, R.C. (2016). R: A language and environment for statistical computing.
Teichroew, J.L., Xu, J., Ahrends, A., Huang, Z.Y., Tan, K. & Xie, Z. (2017). Is China's unparalleled and understudied bee diversity at risk? *Biological Conservation*, 210, 19-28.
Thimmegowda, G.G., Mullen, S., Sottilare, K., Sharma, A., Mohanta, S.S., Brockmann, A. et al. (2020). A field-based quantitative analysis of sublethal effects of air pollution on pollinators. *Proceedings of the National Academy of Sciences*, 117(34), 20653-20661.
Thompson, T. M., Rausch, S., Saari, R. K., & Selin, N. E. (2014). A systems

approach to evaluating the air quality co-benefits of US carbon policies. *Nature Climate Change*, 4(10), 917-923.

Tian, Y., Pan, X., Nishizawa, T., Kobayashi, H., Uno, I., Wang, X. et al. (2018). Variability of depolarization of aerosol particles in the megacity of Beijing: implications for the interaction between anthropogenic pollutants and mineral dust particles. *Atmospheric Chemistry & Physics*, 18, 18203-18217.

Tibesigwa, B., Siikamäki, J., Lokina, R. & Alvsilver, J. (2019). Naturally available wild pollination services have economic value for nature dependent smallholder crop farms in Tanzania. *Scientific Reports*, 9, 3434.

Tong, L., Nieh, J.C. & Tosi, S. (2019). Combined nutritional stress and a new systemic pesticide (flupyradifurone, Sivanto®) reduce bee survival, food consumption, flight success, and thermoregulation. *Chemosphere*, 237, 124408.

Tosi, S., Burgio, G. & Nieh, J.C. (2017). A common neonicotinoid pesticide, thiamethoxam, impairs honey bee flight ability. *Scientific Reports*, 7, 1201.

Touma, D., Stevenson, S., Lehner, F. & Coats, S. (2021). Human-driven greenhouse gas and aerosol emissions cause distinct regional impacts on extreme fire weather. *Nature Communications*, 12, 212.

Uno, I., Eguchi, K., Yumimoto, K., Takemura, T., Shimizu, A., Uematsu, M. et al. (2009). Asian dust transported one full circuit around the globe. *Nature Geoscience*, 2, 557-560.

van Donkelaar, A., Hammer, M.S., Bindle, L., Brauer, M., Brook, J.R., Garay, M.J. et al. (2021). Monthly global estimates of fine particulate matter and their uncertainty. *Environmental Science & Technology*, 55(22), 15287-15300.

Vandyck, T., Keramidas, K., Kitous, A., Spadaro, J. V., Van Dingenen, R., Holland, M., & Saveyn, B. (2018). Air quality co-benefits for human health and agriculture counterbalance costs to meet Paris Agreement pledges. Nature communications, 9(1), 4939. doi:10.1038/s41467-018-06885-9

Vanegas, J., Munoz-Garcia, A., Pérez-Parra, K.A., Figueroa-Galvis, I., Mestanza, O. & Polanía, J. (2019). Effect of salinity on fungal diversity in the rhizosphere of the halophyte Avicennia germinans from a semi-arid mangrove. *Fungal Ecology*, 42, 100855.

Von Frisch, K. (2013). *The dance language and orientation of bees*. Harvard University Press.

Wang, K., Dickinson, R.E. & Liang, S. (2009). Clear sky visibility has decreased over land globally from 1973 to 2007. *Science*, 323(5920), 1468-1470.

Wang, X., Xiao, J., Li, X., Cheng, G., Ma, M., Zhu, G. et al. (2019a). No trends in spring and autumn phenology during the global warming hiatus. *Nature Communications*, 10, 1-10.

Wang, X., Zhang, R. & Yu, W. (2019b). The Effects of PM2.5 Concentrations and Relative Humidity on Atmospheric Visibility in Beijing. *Journal of Geophysical Research: Atmospheres*, 124(4), 2235-2259.

Wells, T., Wolf, S., Nicholls, E., Groll, H., Lim, K.S., Clark, S.J. et al. (2016). Flight performance of actively foraging honey bees is reduced by a common pathogen. *Environmental Microbiology Reports*, 8(5), 728-737.

West, J. J., Smith, S. J., Silva, R. A., Naik, V., Zhang, Y., Adelman, Z. et al.

(2013). Co-benefits of mitigating global greenhouse gas emissions for future air quality and human health. *Nature Climate Change*, 3(10), 885-889.
Wilfert, L., Long, G., Leggett, H.C., Schmid-Hempel, P., Butlin, R., Martin, S.J.M. et al. (2016). Deformed wing virus is a recent global epidemic in honeybees driven by *Varroa* mites. *Science*, 351(6273), 594-597.
Won, W.-S., Oh, R., Lee, W., Kim, K.-Y., Ku, S., Su, P.-C. et al. (2020). Impact of Fine Particulate Matter on Visibility at Incheon International Airport, South Korea. *Aerosol and Air Quality Research*, 1048-1061.
Woodcock, B.A., Bullock, J.M., Shore, R.F., Heard, M.S., Pereira, M.G., Redhead, J. et al. (2017). Country-specific effects of neonicotinoid pesticides on honey bees and wild bees. *Science*, 356, 1393-1395.
Xie, C., Nishizawa, T., Sugimoto, N., Matsui, I. & Wang, Z. (2008). Characteristics of aerosol optical properties in pollution and Asian dust episodes over Beijing, China. *Applied Optics*, 47, 4945-4951.
Xie, Y., Lin, M., Decharme, B., Delire, C., Horowitz, L.W., Lawrence, D.M. et al. (2022). Tripling of western US particulate pollution from wildfires in a warming climate. *Proceedings of the National Academy of Sciences*, 119(14), e2111372119.
Yan, L., Li, Y., Chen, W., Lin, Y., Zhang, F., Wu, T. et al. (2022). Temporal and spatial characteristics of the global skylight polarization vector field. *Remote Sensing*, 14, 2193.
Yao, L., Kong, S., Zheng, H., Chen, N., Zhu, B., Xu, K. et al. (2021). Co-benefits of reducing PM2.5 and improving visibility by COVID-19 lockdown in Wuhan. *NPJ Climate and Atmospheric Science*, 4(1), 40.
Yue, X., Unger, N., Harper, K., Xia, X., Liao, H., Zhu, T. et al. (2017). Ozone and haze pollution weakens net primary productivity in China. *Atmospheric Chemistry & Physics*, 17(9), 6073-6089.
Zeng, J., Han, Q. & Wang, J. (2008). High-spectral resolution simulation of polarization of skylight: Sensitivity to aerosol vertical profile. *Geophysical Research Letters*, 35(20), L20801.
Zhang, Q., Zheng, Y., Tong, D., Shao, M., Wang, S., Zhang, Y. et al. (2019). Drivers of improved PM2. 5 air quality in China from 2013 to 2017. *Proceedings of the National Academy of Sciences*, 116(49), 24463-24469.
Zhang, Q.H., Zhang, J.P. & Xue, H.W. (2010). The challenge of improving visibility in Beijing. *Atmospheric Chemistry & Sciences*, 10(16), 7821-7827.
Zhao, H., Xu, W., Zhang, Y., Li, X., Zhang, H., Xuan, J. et al. (2018). Polarization patterns under different sky conditions and a navigation method based on the symmetry of the AOP map of skylight. *Optics Express*, 26, 28589-28603.
Zheng, C., Zhao, C., Zhu, Y., Wang, Y., Shi, X., Wu, X. et al. (2017). Analysis of influential factors for the relationship between PM2.5 and AOD in Beijing. *Atmospheric Chemistry & Physics*, 17(21), 13473-13489.
박종성, 송인호, 박승명, 신혜정 & 홍유덕 (2015). 서울지역의 PM2. 5 중 OC 와 EC 의 특성및 계절적 변화에 관한 연구. 환경영향평가학회지, 24, 578-592.

국문초록

생태계의 다양한 수분매개곤충 중 벌은 주요 수분매개자로 많은 연구가 이루어져 왔다. 그러나 지난 수십 년간 생물학적·비생물학적 원인들로 전지구적 벌 개채수가 계속해서 감소하고 있다. 이러한 경향에 먹이자원의 감소, 서식지 파괴, 살충제 사용과 같은 인위적 스트레스의 증가가 벌 개체수 및 벌의 채이 활동에 영향을 미치는 원인으로 지목되어 연구되고 있다. 여기에 대기질의 저하 또한 벌의 채이 활동을 방해할 수 있다. 대기 중 미세먼지의 증가는 태양빛 중 전자기파의 과도한 산란을 일으키고 이는 빛의 선형편광도 감소로 이어진다. 서양꿀벌(*Apis mellifera*)은 태양 주변에 나타나는 선형편광에 담긴 광학적 정보를 활용하여 비행한다. 그러나 꿀벌이 이러한 광학적 정보를 비행에 활용하기 위해서는 최소 15%의 선형편광도(Degree of linear polarization, DoLP)가 기반되어야 한다.

대부분의 대기 중 입자상 에어로졸의 질량 산란 효율은 직경이 큰 입자보다 직경이 1 μm 미만인 입자에서 크다. 따라서, PM2.5(직경이 2.5 μm 이하인 입자)로 나타내어지는 초미세먼지의 농도는 DoLP와 상관성이 있다. 결과적으로 PM2.5 질량농도 증가에 따른 DoLP의 감소는 꿀벌의 시계를 제한함으로써 채이 활동 효율을 저하시킬 수 있다. 그러나 대기질의 저하가 실제 꿀벌의 채이 활동에 어떤 영향을 주는지에 대한 경험적 증거가 부족했다. 이 연구는 대기 중 PM2.5 질량농도와 DoLP 사이의 상관관계를 밝히고, PM2.5 증가에 따른 꿀벌 시계 제한의 시·공간적 규모를 예측하는 것을 목표로 한다.

무선주파수인식장치를 활용하여 꿀벌 군집의 채이 활동을 모니터링 함으로써 대기 중 고농도 미세먼지 발생 시의 꿀벌의 평균 채이 시간을 저농도 미세먼지 발생 시의 평균과 비교할 수 있었다. 고농도 미세먼지 발생 시의 꿀벌의 채이 시간은 그렇지 않은 경우보다 평균 71% 증가하였다. 또한, 대기 중 미세먼지 농도가 다시 낮아졌을 때 채이 시간이 그 이전의 수준으로 회복되지 않았다. 그러나, 모니터링 결과를 바탕으로 구축한 선형 모형을 통해, 고농도 미세먼지 발생과 상관없이 PM2.5 질량농도의 증가가 꿀벌 채이 시간을 지수적으로 감소시킴을 분석하였다. 입자의 모양을 설명하여 발생 기원을 구분할 수 있게

해주는 광학적 지표인 편광소멸도(depolarization ratio)를 변수로 한 통계 분석에서 대기 중에 황사 입자와 같은 비구형의 입자가 많은 날보다 일반적인 도심 오염물질이 더 압도적인 경우 PM2.5 질량농도의 DoLP 감소에 대한 효과가 훨씬 더 큰 것으로 분석되었다. 이러한 실제 필드에서의 모니터링 결과가 갖는 중요한 이유는, 늘어난 비행 시간으로 꿀벌이 살충제나 해충과 같은 다른 스트레스 원인들에 노출될 확률을 높아지기 때문이다.

필드에서의 경험적 증거를 토대로 PM2.5 증가에 따른 꿀벌 시계 제한의 시·공간적 규모의 잠재적 증가를 분석하기 위해 지상관측과 미래 예측으로 이루어진 종합적인 연구를 수행하였다. 우선, 장기간의 편광 지상관측을 통해 PM2.5 질량농도와 DoLP 사이의 상관관계를 정량화하였다. Digital all-sky imaging polarimetry system을 활용하여 2018-2019년, 2020-2021년의 기간동안 편광 관측을 수행하였다. 이후 전천 촬영물에 대해 스토크스 매개변수를 사용하여 DoLP를 산출하였다. PM2.5 질량농도와 DoLP 사이의 상관관계를 모수화함으로써 전체 하늘의 DoLP를 꿀벌이 비행에 사용할 수 있는 최소한의 DoLP(15%) 이하로 감소시키는 PM2.5의 임계 질량농도를 산출할 수 있었다. 꿀벌과 선형편광도에 관련한 연구는 전체 하늘에 나타나는 다양한 DoLP 값 중 최대 DoLP에 대해서만 이루어져 왔으나, 구름과 같은 영향으로 실제 꿀벌이 비행 중 직면하는 하늘에 항상 DoLP의 최대값이 분포하는 것은 아니다. 따라서 이 연구에서는 최대 DoLP와 평균 DoLP 두가지 경우를 나누어 임계 PM2.5 질량농도를 산출하였다. 즉, 일정 PM2.5 질량농도에 있어 꿀벌의 비행 중 전체 하늘에 나타나는 DoLP는 이 최대값과 평균값 사이에 놓이게 된다.

앞서 산출한 PM2.5 임계 질량농도를 ECHAM5/MESSy 대기 기후 화학 모형이 모의한 2050년 전지구 PM2.5 예측값에 투영하였다. 이 모형은 대기질 개선을 위한 노력이 2010년 수준에 머무를 것이라고 가정하고 2050년의 지역별 인구 증가 및 경제적 성장을 기반으로 미래의 대기질을 모의한다. 이러한 모형에의 투영을 통해 꿀벌이 시계 제한을 경험할 것으로 예측되는 고위험지역(risk hotspot)을 확인하고, 2050년 꿀벌 시계 제한의 시공간적 규모를 분석하였다. 분석 결과, 인도와 중국에서 꿀벌 시계 제한의 시·공간적 규모 증가가 가장 클 것으로 나타났다. 보수적인 상한계 추정임에도 불구하고, 인도는 꿀벌 시계 제한의 빈도가

1일 이상 늘어나는 고위험지역이 2010년 0.06 백만 km^2 수준에서 2050년 0.75백만 km^2로 크게 증가할 것으로 추정되었다. 한 편, 중국에서는 2050년 고위험지역이 2백만 km^2에 걸쳐 분포하는 것으로 추정되었는데 이 중 1.1백만 km^2의 지역에서 2010년 대비 시계 제한의 빈도가 최소 1일 이상 증가하는 것으로 분석되었다.

대기 중 미세먼지 증가에 기인한 꿀벌의 시계 제한과 이에 따른 벌의 채이 시간의 증가는 앞서 연구된 기타 인위적 스트레스 요인에 더불어 식물-수분매개자 간 관계를 위협하는 주요 인자가 될 수 있다. 종합적으로, 이 학위논문의 연구결과는 식물-수분매개자 간 상호작용를 보호함에 있어 대기오염 완화의 중요성을 강조하고 있다.

주요어: 생물다양성, 수분서비스, 꿀벌, PM2.5, 선형편광도, 대기질 예측
학번: 2015-31317